XIII. Phreatophytes

XIII. Phreatophytes

a. Detecting the Changes of the Phreatophyte Evapotranspiration on the South Platte Using Remote Sensing and Weather Data

Table of Contents

a. Detecting the Changes of the Phreatophyte Evapotranspiration on the South Platte Using Remote Sensing and Weather Data 2

b. Using Surface Energy Balance-Based Model to Estimate the Evapotranspiration of the Irrigated Crops and Phreatophytes of the South Platte River Basin..... 44

List of Figures

Figure 13.1. South Platte weather stations. 9

Figure 13.2. The reaches of the South Platte. 10

Figure 13.3. An example of DOS correction for band 3 for the 32/32 scene of Landsat 5 for 2010 using histograms. 14

Figure 13.4. Examples of the cumulative distribution functions (CDFs) of the row data of NDVI and the stretched NDVI* of the three 2001 scene images. 18

Figure 13.5. Landsat 5 2010 and NAIP aerial photos natural color 2011 used to track the changes of phreatophytes in reach # 13. 19

Figure 13.6. Annual and seasonal ET and precipitation data from 81 weather stations using the 30 year average (1981 - 2010) acquired from the National Climate Center Data (NCDC). 21

Figure 13.7. Semi-variograms of different datasets used to krig the annual and seasonal reference ET and precipitation data. 21

Figure 13.8. Developed maps for the annual and seasonal ET and precipitation data from 81 weather stations using the 30 year average (1981 - 2010) acquired from the National Climate Center Data (NCDC). 23

Figure 13.9. The developed annual and seasonal ET minus precipitation from weather station data. 25

Figure 13.10. Flowchart summarizing the procedure for creating ET_g from Landsat 5 satellite images, weather data (reference ET and precipitation), and aerial photos..... 26

Figure 13.11. Comparison among the years 1990, 2010, and 2010 of the annual and seasonal phreatophyte ET (AcreFT). 28

Figure 13.12. An example of using the dendrogram as a grouping tool technique. 31

Figure 13.13. Applying grouping tool techniques: (a) before setting the target classes, (b) after setting the target classes. 33

Figure 13.14. Applying grouping tool techniques. 34

Figure 13.15. Comparison between the combined annual and seasonal phreatophyte ET_g (AcreFT) and the separated of the perennial from the annual for 2010. 36

Figure 13.16. Digital Elevation Model (DEM) of the study area. 55

Figure 13.17. Irrigated Parcels of 2010 and phreatophyte shapefiles. 56

Figure 13.18. Weather stations, hourly *ET* (mm), and daily *ET* (mm) developed from weather stations. . 58

Figure 13.19. Examples of cold and hot points displayed on surface temperature raster on the left and on the original landsat 5 image. 61

Figure 13.20. Example of ReSET model output: (a) individual *ET* raster generated from single image, (b) interpolation of *ET* rasters of the whole season, (c) the final *ET* raster of the whole season from one scene. 63

Figure 13.21. Comparison of the percentages of the *ET* of all irrigated crops for the years 2001 and 2010 of the South Platte River Basin. 65

List of Tables

Table 13.1. Description of the acquired Landsat 5 images acquired from the header files of the scenes. . 11

Table 13.2. Values of $LMIN_\lambda$, $LMAX_\lambda$, and $ESUN_\lambda$ adopted from Chander et. al., 2007. 13

Table 13.3. DOS correction values for the Landsat 5 sconces for all images. 16

Table 13.4. Statistics of the annual and seasonal ET and precipitation data from 81 weather stations using the 30 year average (1981 - 2010) acquired from the National Climate Center Data (NCDC)..... 20

Table 13.5. Prediction errors of the different models 22

Table 13.6. Comparison among the years 1990, 2001, and 2010 of the annual and seasonal phreatophyte ET (AcreFT)..... 27

Table 13.7. Comparison between the combined annual and seasonal phreatophyte ET_g (AcreFT) and the separated of the perennial from the annual for 2010. 35

Table 13.8. Landsat 5/7 scenes ID and acquisition dates..... 53

Table 13.9. Areas of different crops and phreatophytes of 2001 and 2010 59

Table 13.10. The area and ET of all irrigated crops and phreatophyte of the South Platte River Basin. ... 66

Detecting the Changes of the Phreatophyte Evapotranspiration on the South Platte Using Remote Sensing and Weather Data

Abstract

This study investigates the development of phreatophyte evapotranspiration from groundwater (ET_g). The stretched normalized difference vegetation index (NDVI*) developed from Landsat 5 satellite images and weather station data (reference ET and precipitation) are used to estimate the phreatophyte ET_g. Aerial photos are used to help identify the perennial from the annual phreatophytes in the developed NDVI*. Two approaches are used in this study to estimate the phreatophyte ET_g. The first is to use the NDVI* that was developed form Landsat 5 images with the annual weather data to estimate phreatophyte ET_g without separating the annual from perennial. The second is an enhancement of the first approach by adding high resolution aerial photos to help separate perennial and annual phreatophytes. With the second approach, annual weather data is used with the NDVI* to generate perennial phreatophyte ET_g, while seasonal weather data is used with the NDVI* to generate seasonal phreatophyte ET_g. The objectives of this study are: 1) to estimate the ET_g used by the phreatophyte in the South Platte region, 2) to estimate the magnitude of ET_g used by each of the annual and perennial phreatophytes, 3) to track the changes of both the annual and perennial phreatophytes over a selected period of time—1990 to 2010, and 4) to provide guidelines for decision makers to control the phreatophytes of the South Platte for better management of ET_g. Landsat 5 satellite images with a 30-meter resolution were acquired for the years 1990, 2001, and 2010. The resolution of the Landsat 5 images makes it difficult to differentiate between annual and perennial phreatophytes; therefore, aerial photos with high resolution were also collected. Color aerial photos were acquired for the year 2011 from the National Agricultural Imagery Program

(NAIP) with one-meter resolution. Weather station data, reference ET, and precipitation data were collected from 81 weather stations scattered over the South Platte. The thirty year average (1981 - 2010) of both annual and seasonal ET_g and precipitation were considered. Seasonal and annual weather data were used with the NDVI* to estimate the annual and perennial phreatophyte ET_g respectively in a raster map format. Techniques including unsupervised classification and grouping tools were used to separate and quantify both the annual and perennial phreatophytes from the developed raster maps. The first approach shows that the phreatophytes in general increased from 1990 to 2010. The increase from 1990 to 2001 was slight for most of the reaches and there was a decrease in some reaches. However, there was an increase from 1990 to 2010 in all reaches. When applying the second approach to 2010 data, the ET_g resulting from annual phreatophytes is less than that of the seasonal. Also, the second approach shows that the ET_g resulting from the combined annual and perennial phreatophytes is less than the combined phreatophyte results from the first approach.

Introduction

Remote sensing can offer practical approaches for evapotranspiration (ET) estimation. A normalized difference vegetation index (NDVI) is capable of estimating ET (Kerr et al., 1989; Chong et al., 1993; Kustas et al., 1994; Seevers and Ottmann, 1994; Szilagyi et al., 1998; Szilagyi, 2000, 2002). Baugh and Groeneveld (2006) and Groeneveld and Baugh (2007) show that NDVI provides greatly improved prediction after conversion to stretched NDVI (NDVI*), a process that removes non-systematic variation. NDVI is an indicator of vegetation vigor often used to measure environmental response to landscape-scale hydrology, including rainfall (Wang et al., 2003; Ji and Peters, 2003) and ET (Kerr et al., 1989; Chong et al., 1993; Kustas et al.,

1994; Seevers and Ottmann, 1994; Szilagyi et al., 1998; Szilagyi, 2000, 2002). A linear relationship (r^2= 0.85) was found by Wang et al. (2003) between average growing season NDVI and precipitation for the Great Plains, USA. Also in the North American Great Plains, Yang et al. (1998) report a linear relationship between precipitation and NDVI (r^2= 0.63), and Ji and Peters (2003) optimized a linear relationship between the standard precipitation index (SPI) and NDVI using a three-month averaging period. Malo and Nicholson (1990) found a linear relationship between precipitation and NDVI in the Sahel. In regions where precipitation is limited, Tucker and Nicholson (1999) found NDVI to be related to annually integrated precipitation. Kawabata et al. (2001) reported linear relationships between annual precipitation and NDVI in northern Australia (r^2= 0.75) and Argentina (r^2=0.54). Baugh and Groeneveld (2006) evaluated the NDVI against all published vegetation indices and found that it was superior to all other indices for predicting a linear relationship between vegetation growth and antecedent precipitation. NDVI can be used to track plant response to downward adjustment of water tables due to groundwater pumping or recovery due to increased recharge. Modeling packages such as MODFLOW (Harbaugh et al., 2000; McDonald and Harbaugh, 2003) contain algorithms to adjust ET as the depth to water changes; however, such relationships remain largely unverified.

Several studies have been conducted to estimate phreatophyte ET_g; however, the majority of them lacked accuracy. This was due to the fact that most solely relied on the Landsat images, which have 30m*30m resolution. This low resolution does not allow an accurate estimate of the phreatophytes; in particular, the perennial phreatophytes. In addition, most of the previous studies used few weather station data, causing less accuracy in the interpolation. The main contribution of this study is that it combines the advantages of both Landsat images and the aerial photos. The advantage of Landsat is that it includes the red and near infrared bands.

Chlorophyll—responsible for the green color of plants—absorbs red light, while leaf tissue is highly reflective in the near infrared. Therefore, the NDVI developed from the red and infrared is a good indicator of vegetation vigor. However, the disadvantage of the Landsat is the low resolution of the images. The study utilizes the aerial photos with 1m*1m resolution to fill in the gap of the landsat images by separating the annual and perennial phreatophytes. Another contribution of this study is that it uses data from 81 weather stations, improving interpolation of the weather data.

The Study Area

Figure 13.1 shows the South Platte River and the weather stations located near the river. The South Platte River is the primary water supply for the Denver metro area. It is one of the two principal tributaries of the Platte River, and its drainage basin includes most of the eastern side of the Rocky Mountains in Colorado, most of the Colorado Front Range and Eastern Plains, and a portion of southeastern Wyoming. It joins the North Platte River in western Nebraska to form the Platte, which then flows across Nebraska to the Missouri River. The South Platte serves as the principal source of water for eastern Colorado. Figure 1 shows that more than eighty weather stations are scattered along the river—these stations have collected weather data since 1950.

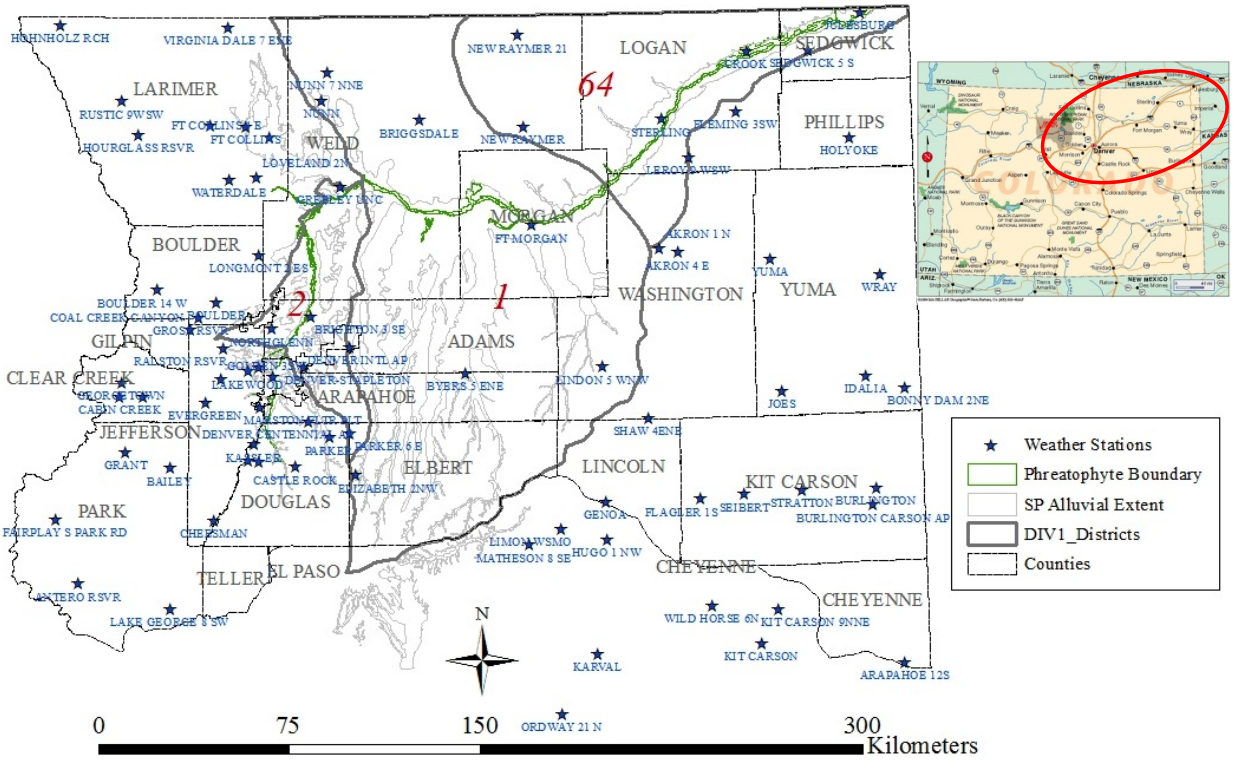

Figure 13.1. South Platte weather stations.

In order to track the spatial variability of the phreatophyte ET_g of the South Platte, the main stream of the river was divided into 13 reaches as shown in Figure 2. These reaches were used at the stream gages and diversion points. The Figure shows the reach number as well as the name of the gage or diversion. The reaches follow the same order that was used by Groeneveld et. al., 2007, to allow a comparison of the findings of this study with Groeneveld et. al., 2007.

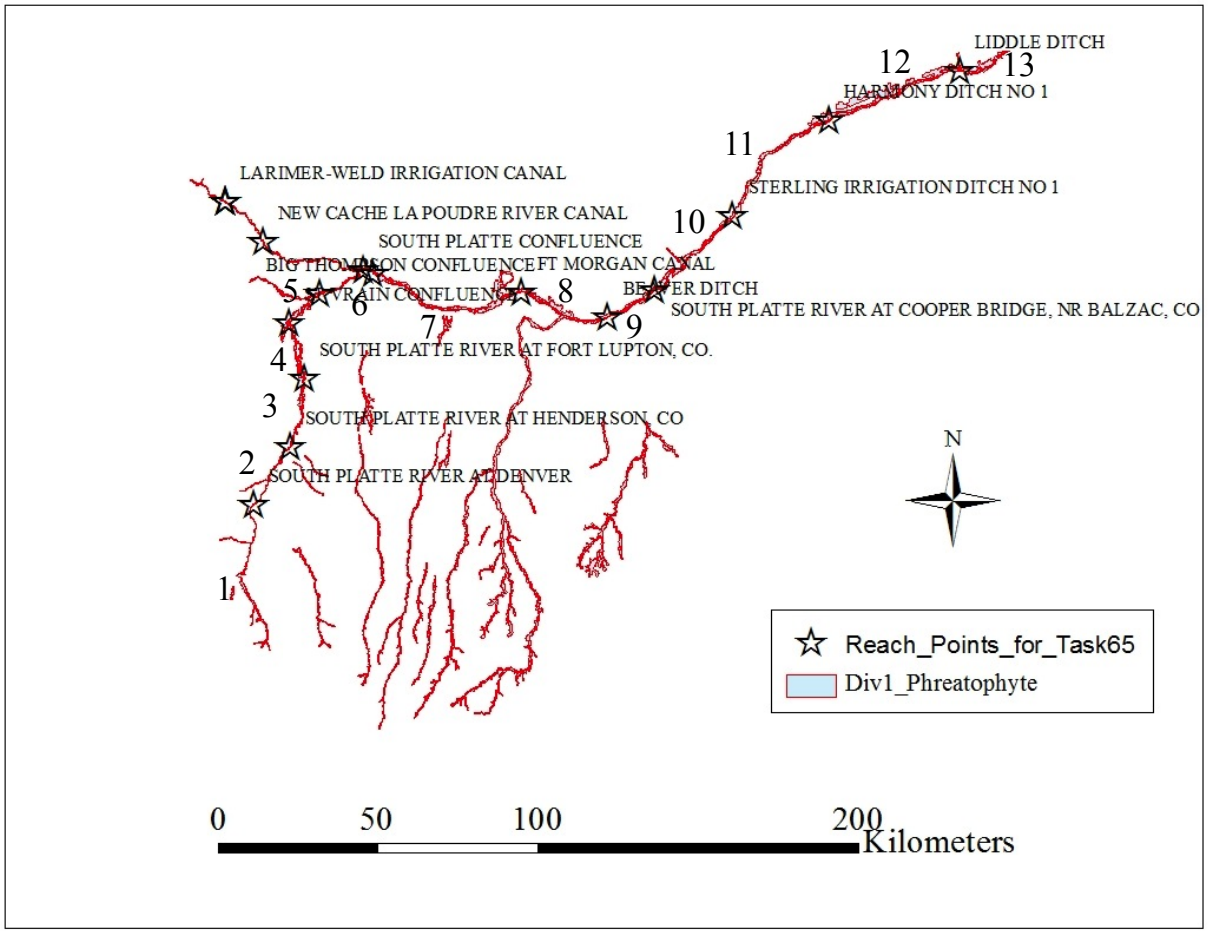

Figure 13.2. The reaches of the South Platte.

Data Collection and Preparation

Acquired Landsat Images

In order to track the changes of the South Platte phreatophyte ET_g, long time scales are needed due to the phreatophytes' slow growth rate. Therefore, sets of images were acquired for the years 1990, 2001, and 2010 to be investigated for changes in the phreatophytes. The study area was overlaid by three Landsat 5 satellite scenes with the following paths/rows, which allows location of the image: 32/32, 33/32, and 33/33. The Landsat 5 images were acquired based on the

following criteria: 1) no cloud cover or strips (caused by failure of the scan line corrector) that obscure the study area, 2) images were acquired during the peak of the summer season to guarantee that the ET can reach it maximum during the season, and 3) for each individual year, time difference of images acquisition dates should not exceed one or two weeks to guarantee no significant changes in phreatophyte growth among the three images of any individual year. Table 1 shows the acquired images for the years 1990, 2001, and 2010 of the Landsat with Space Aircraft #5 and Thematic Mapper (TM) sensor ID.

Table 13.1. Description of the acquired Landsat 5 images acquired from the header files of the scenes.

Landsat Scene ID	Path/Row	Acquisition date	θ_s
LT50320321990183XXX03	32/32	July 2, 1990	58.74
LT50330321990174XXX06	33/32	June 23, 1990	59.33
LT50330331990174XXX05	33/33	June 23, 1990	59.63
LT50320322001197LGS01	32/32	July 16, 2001	60.56
LT50330322001188LGS02	33/32	July 7, 2001	61.64
LT50330332001188LGS02	33/33	July 7, 2001	62.12
LT50320322010174EDC00	32/32	June 23, 2010	64.41
LT50330322010181EDC00	33/32	June 30, 2010	63.97
LT50330332010181EDC00	33/33	June 30, 2010	64.52

Landsat Images Preparation

Correction for Reflectance

The Landsat TM and Enhanced (ETM+) sensors acquire temperature data and store this information as a digital number (DN) with a range between zero and 255. Satellites measure radiance rather than reflectance. Reflectance is the ratio of the reflected light measured at the satellite divided by incoming solar radiation. The pattern of radiance across the satellite bands is often similar to the pattern of reflectance across the same bands, but satellite radiance is altered

by atmospheric effects. Reflectance is important because it incorporates calculations that correct for sensor differences and for the strength of solar radiation that is slightly influenced by the time of the year. Therefore, before generating the NDVI or creating masks for water bodies from Landsat, the DN should be converted into reflectance. Images can be processed to reflectance using header data packaged with each satellite scene (Chander and Markham, 2003; Chander et al. 2007). There are two steps to convert the DN to reflectance: the DN needs to be converted to radiance, then the radiance needs to be converted to reflectance. For relatively clear Landsat scenes, a reduction in between-scene variability can be achieved through a normalization of solar irradiance by converting spectral radiance to planetary reflectance or albedo. There are two advantages for using reflectance rather than radiance: 1) the cosine effect of different solar zenith angles due to the time difference between data acquisition can be removed, and 2) it compensates for different values of exoatmospheric solar irradiances arising from spectral band differences. The following conversion equations are used:

Converting DN to Radiance (L_λ)

$$L_\lambda = G_{\text{rescale}} \times Q_{\text{cal}} \times B_{\text{rescale}}$$

where:

L_λ : Spectral radiance at the sensor's aperture [W/(m^2.sr.μm)]

$G_{rescale}$: Band - specific rescaling gain factor $\left[\left(\text{W}/\left(\text{m}^2.sr.\mu m\right)\right)/DN\right]$

$$G_{\text{rescale}} = \left(\frac{LMAX_\lambda - LMIN_\lambda}{Q_{\text{calmax}} - Q_{\text{calmin}}}\right) = \left(\frac{LMAX_\lambda - LMIN_\lambda}{255}\right)$$

$LMIN_\lambda$: Spectral radiance that is scaled to $Q_{cal\,\min}$ [W/(m^2 . sr. μm)]

$LMAX_\lambda$: Spectral radiance that is scaled to $Q_{cal\,\max}$ [W/(m^2 . sr. μm)]

$Q_{cal\max} = 255$ $Q_{cal\min} = 0$

$B_{\text{rescale}} = LMIN_\lambda$: Band - specific rescaling bias factor $\left[\text{W}/\left(\text{m}^2 .sr.\mu m\right)\right]$

Q_{cal} : Quantized calibrated pixel value *[DN]*

$Q_{cal\min}$: Minimum quantized caliberated pixel value *(DN = 0)* corresponding to $LMIN_\lambda$

$Q_{cal\max}$: Maximum quantized caliberated pixel value *(DN = 255)* corresponding to $LMAX_\lambda$

Converting the Radiance (L_λ) to Reflectance (ρ_p)

$$\rho_p = \frac{\pi L_\lambda d^2}{ESUN_\lambda \cos\theta_s}$$

where:

ρ_p: Unitless planetary reflectance

$ESUN_\lambda$: ESUNMean solar exoatmospheric irradiances

θ_s : Solar zenith angle in degrees (Values are provided in Table 1 because each scene with all bands has one angle)

Table 13.2. Values of $LMIN_\lambda$, $LMAX_\lambda$, and $ESUN_\lambda$ adopted from Chander et. al., 2007.

Band #	$B_{\text{rescale}} = LMIN_\lambda$ (W/(m^2 . sr. µm))	$LMAX_\lambda$ (W/(m^2 . sr. µm))	$ESUN_\lambda$ (W/(m^2 . µm))
1990 images			
3	-1.17	204.30	1557
4	-1.51	206.20	1047
5	-0.37	27.19	219.3
2001 images			
3	-1.17	204.30	1557
4	-1.51	206.20	1047
5	-0.37	27.19	219.3
2010 images			
3	-1.17	264.0	1557
4	-1.51	221.0	1047
5	-0.37	30.2	219.3

Correction for Dark Object Saturation (DOS)

Dark Object Saturation (DOS) is used to minimize data scatter associated with local atmospheric conditions at the time of the satellite overpass. The correction of atmospheric scattering is often called haze. Various methods to correct or remove the additive haze component have been developed, including the widely used dark-object subtraction technique. A problem with most of these methods is that the haze values for each spectral band are selected independently (Chavez, 1988). This can create problems, because atmospheric scattering is highly wavelength-dependent in the visible part of the electromagnetic spectrum, and the scattering values are correlated with each other. Therefore, multispectral data such as from Landsat TM must be corrected with haze values that are spectral dependent (Chavez, 1988). The improved dark-object subtraction technique allows the user to select a relative atmospheric scatter model to predict the haze values for all the spectral bands from a selected scattering band haze value. The improved method normalizes the predicted haze values for the different gain and offset parameters used by the imaging system.

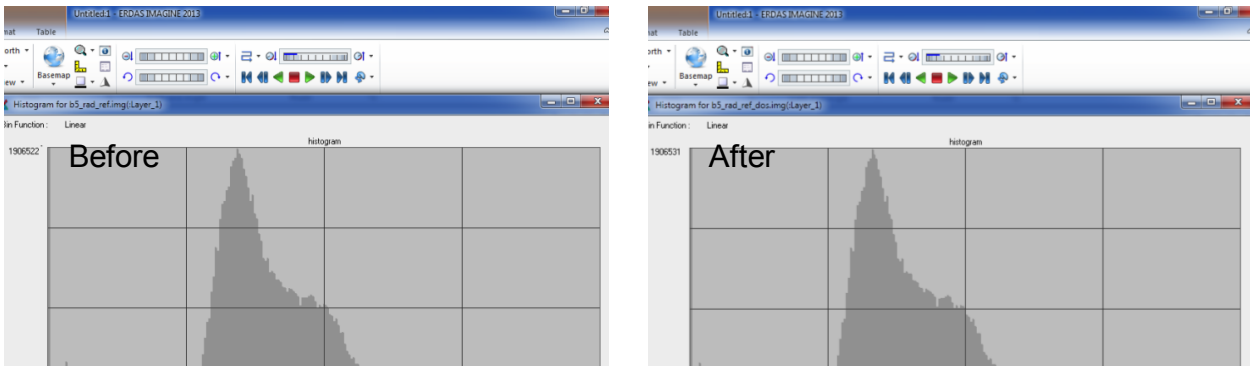

Figure 13.3. An example of DOS correction for band 3 for the 32/32 scene of Landsat 5 for 2010 using histograms.

Figure 13.3 shows DOS correction for band 3 for the 32/32 scene of Landsat 5 for the year 2010. Looking at the left part of the two histograms, the processing of the DOS subtracted a portion form the histogram on the left hand side to generate the histogram on the right hand side. In order to perform the improved dark-object subtraction technique, the subtracted value from band 3 is considered as a selected scattering band haze value. This selected value is used with the selected relative atmospheric scatter model to predict the haze values for all the spectral bands.

Table 13.3. DOS correction values for the Landsat 5 sconces for all images.

Band #	GAIN	OFFSET	Normalized Gain	MFM	SHV	DOS values
07/02/1990 (32_32)						
3	0.9215	-1.17	1.00	1.000	13.25	12.08
4	1.082	-1.51	1.17	0.400		5.67
5	7.9967	-0.37	8.68	0.026		2.73
06/23/1990 (32_32)						
3	0.9216	-1.17	1.00	1.000	13.00	11.83
4	1.082	-1.51	1.17	0.400		5.56
5	8.0927	-0.37	8.78	0.026		2.70
06/23/1990 (32_32)						
3	0.9216	-1.17	1.00	1.000	13.00	11.83
4	1.082	-1.51	1.17	0.400		5.56
5	8.0927	-0.37	8.78	0.026		2.70
07/16/2001 (32_32)						
3	0.9041	-1.17	1.00	1.000	13.00	11.83
4	1.082	-1.51	1.20	0.400		4.15
5	8.1165	-0.37	8.98	0.026		2.39
07/07/2001(33_32)						
3	0.9042	-1.17	1.00	1.000	12.00	10.83
4	1.082	-1.51	1.20	0.400		5.58
5	8.1469	-0.37	9.01	0.026		2.56
07/07/2001 (33_33)						
3	0.9042	-1.17	1.00	1.000	13.00	11.83
4	1.082	-1.51	1.20	0.400		4.15
5	8.1469	-0.37	9.01	0.026		2.40
06/23/2010 (32_32)						
3	0.903	-1.17	1.00	1.000	14.00	12.83
4	1.082	-1.51	1.20	0.400		4.64
5	8.2345	-0.37	9.12	0.026		2.67
06/30/2010 (33_32)						
3	0.903	-1.17	1.00	1.000	12.00	10.83
4	1.082	-1.51	1.20	0.400		3.68
5	8.2339	-0.37	9.12	0.026		2.20
06/30/2010 (33_33)						
3	0.903	-1.17	1.00	1.000	14.00	12.83
4	1.082	-1.51	1.20	0.400		4.64
5	8.2339	-0.37	9.12	0.026		2.67

The DN values for DOS can be calculated as follows:

$$\mathrm{DN(HAZE)_i} = (\text{SHV of a chosen band}) * (\mathrm{MFM})_i * (\mathrm{GNF})_i + Offset_i$$

Table 3 shows the DOS correction values for the Landsat 5 sconces for all the acquired images. The Gain values were obtained from the calibration parameter file (CPF), the OFFSET values were obtained from the metadata file of each image, and the Multiple Factor Model (MFM) was adopted from Chavez, 1988. The Gain was normalized for band 3 and the very clear haze model, a relative scattering model, was selected with the MFM values shown in the table. In order to avoid independence among different bands spectral values, a start haze value (SHV) is selected; for example, band 3 for the scene 32/32 of July 2, 1990. The DOS values for all bands are obtained by multiplying the normalized Gain value with the MFM value and the SHV of band3, and then adding the offset values for each band to the resulting value.

Normalized Differencing Index (NDVI) and Stretched NDVI, NDVI*

NDVI utilizes the difference in two adjacent bands in the red and near-infrared portion of the spectrum that occurs when viewing healthy vegetation. Chlorophyll, responsible for the green color of plants, absorbs red light, while leaf tissue is highly reflective in the near infrared (Buschmann and Nagel, 1993). NDVI is calculated by subtracting the response in the red band (TM Band 3) from the reflectance in the near-infrared band (NIR; TM Band 4) and then dividing the sum of the reflectances for these two bands (Rouse et al., 1974).

$$NDVI = \frac{(Band4 - Band3)}{(Band4 + Band3)}$$

Another derivation for NDVI is needed to eliminate the non-systematic variation of the NDVI that stretches the NDVI distribution for vegetation from zero to one (Groeneveld and Baugh, 2007). The resulting stretched NDVI is NDVI*, and its functionality is the same as the crop coefficient (*kc*), since NDVI* is a scalar value for multiplication by actual ET_o (Allen et al., 1998).

$$NDVI_i^* = \frac{(NDVI_i - NDVI_o)}{(NDVI_s - NDVI_o)}$$

Examples of values of the $NDVI_o$ and $NDVI_s$ are shown on the upper right side of Figure 3 for the three scenes of 2001.

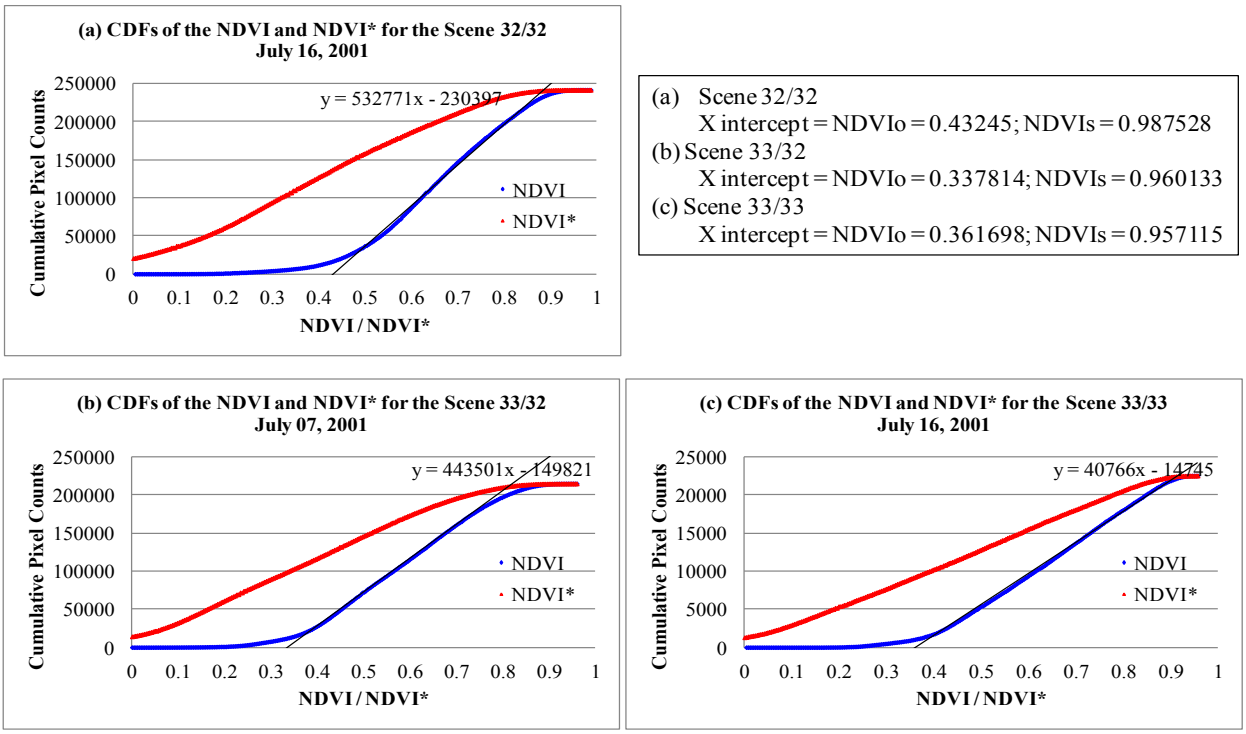

Figure 13.4. Examples of the cumulative distribution functions (CDFs) of the row data of NDVI and the stretched NDVI* of the three 2001 scene images.

Figure 4 shows three examples of cumulative distribution functions (CDF) of the three scenes from the images acquired in 2001 in which $NDVI_o$ is predicted using linear regression function as well as NDVI*. After subtraction, the lower tail of the curve below $NDVI_o$ yields a small set of negative values that were set to zero to avoid creating negative values for ET. Very low values of NDVI, often less than zero, also generally occur for clear open water in most TM scenes and scene subsets. The figure shows how the extreme variations in NDVI while calculating NDVI* enable viewing an orderly progression of the CDFs. The orderly progression

of NDVI* represented a significant enhancement of the signal for vegetation response to antecedent precipitation.

Acquired Aerial Photos:

The NDVI* can be developed efficiently using the Landsat 5 satellite images; however, it is difficult to distinguish or delineate the different species of phreatophyte due to the resolution of Landsat 5, 30 meters. Therefore, high resolution aerial photos were acquired to fill the gap of low resolution of Landsat 5 images. Color aerial photos were acquired for the year 2011 from the National Agricultural Imagery Program (NAIP) with one-meter resolution. These photos are 1 meter resolution and county based mosaic. Figure 5 shows the difference in resolution between Landsat 5 and aerial photos and how the high resolution of the aerial photos can be used to differentiate between the annual (trees) and perennial (grass or vegetation) types of phreatophyte.

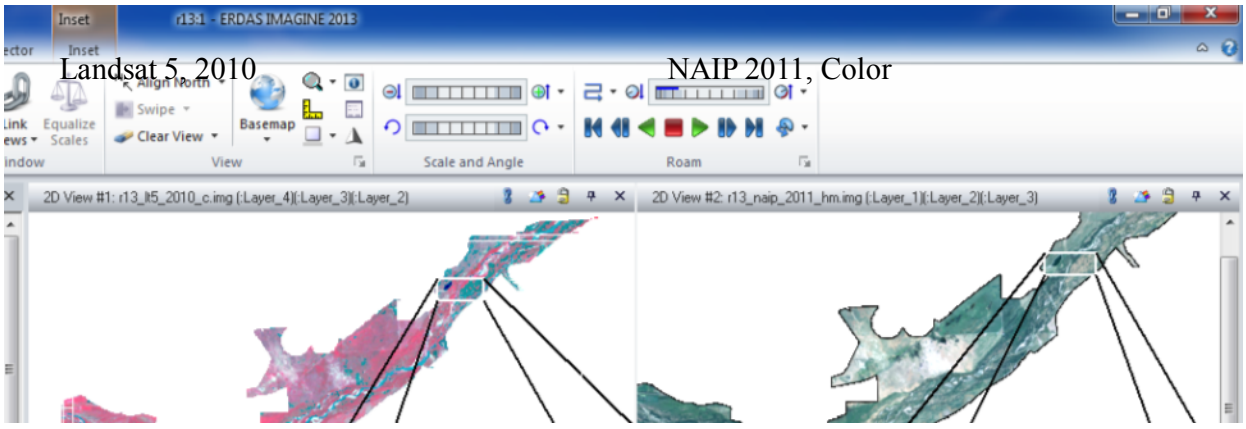

Figure 13.5. Landsat 5 2010 and NAIP aerial photos natural color 2011 used to track the changes of phreatophytes in reach # 13.

Acquiring Weather Data

Weather data were acquired from the National Climate Center Data (NCDC). The 30-year averages (1981 - 2010) were considered for 81 stations around the South Platte. Table 13.4

shows the statistics of the annual and seasonal reference ET and precipitation. The values of minimum, maximum, mean, and standard deviation shown in Table 13.4 indicate that the data are homogeneous with few outliers. In geostatistical analysis, the number of interpolated points should be large enough to generate accurate maps. All 81 weather stations' data were kept for interpolation, especially the values of the points far away from the alluvial extent of the South Platte not represented by either the maximum or minimum values, i.e., not outliers. The existence of all data will improve the interpolation.

Table 13.4. Statistics of the annual and seasonal ET and precipitation data from 81 weather stations using the 30 year average (1981 - 2010) acquired from the National Climate Center Data (NCDC).

Dataset	Min. (in)	Max. (in)	Mean (in)	Std. Dev (in)	Median (in)
Annual ET	34.75	54.78	49.34	4.79	50.94
Annual Precipitation	10.86	30.82	17.41	3.09	17.12
Seasonal ET	22.65	33.47	30.60	2.69	31.60
Seasonal Precipitation	7.43	14.18	10.65	1.49	10.66

Blaney-Criddle (temperature based equation) was used to calculate the reference ET. The Blaney–Criddle equation is a relatively simplistic method for calculating ET; however, it is ideal when only air temperature data is available for a site. The Blaney-Criddle equation is as follows:

$ET_o = p \cdot (0.46 \cdot T_{mean} + 8)$

where

ET_o is the reference evapotranspiration [mm/day] (monthly)

T_{mean} is the mean daily temperature [°C] given as $T_{mean} = (T_{max} + T_{min})/2$

p is the mean daily percentage of annual daytime hours

The term "reference" refers to the ET equations calibrated to estimate the water use of a well-watered alfalfa or grass field under a set of local weather conditions.

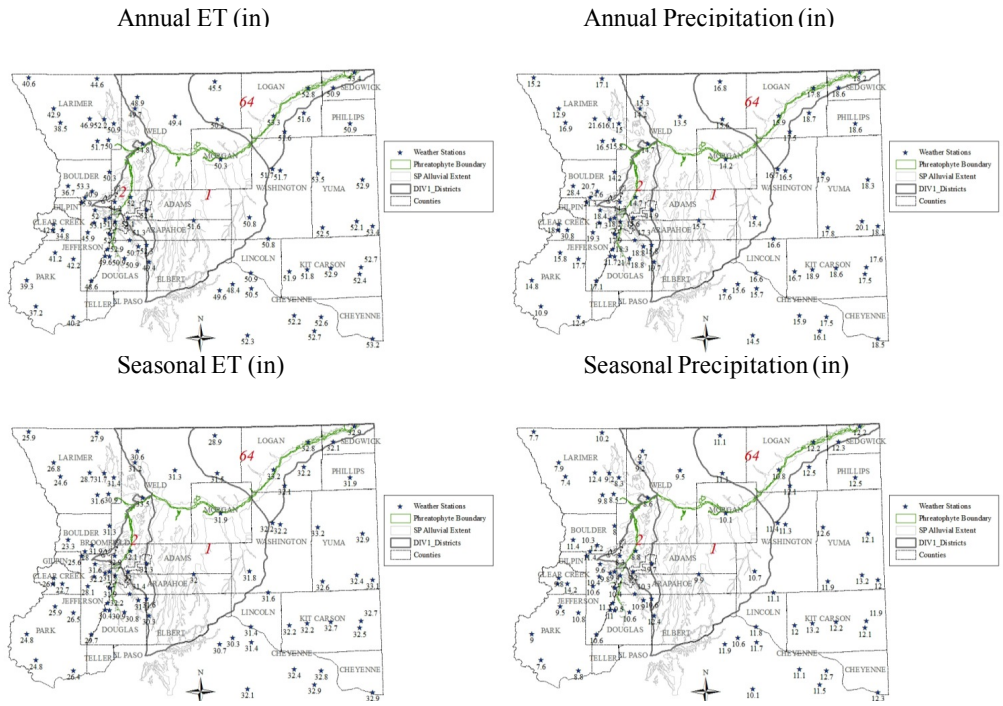

Figure 13.6. Annual and seasonal ET and precipitation data from 81 weather stations using the 30 year average (1981 - 2010) acquired from the National Climate Center Data (NCDC).

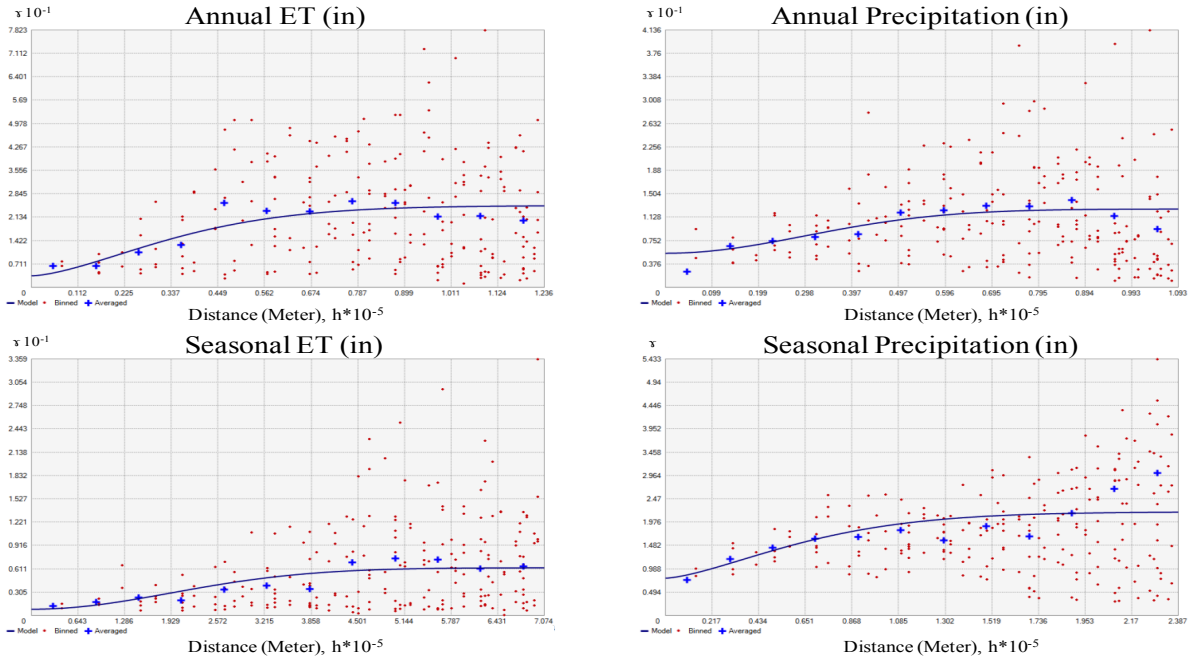

Figure 13.7. Semi-variograms of different datasets used to krig the annual and seasonal reference ET and precipitation data.

Figure 13.7 shows the Semi-variograms of different datasets used to krig the annual and seasonal reference ET and precipitation data. Cross-validation statistics were used to evaluate the variogram models. Cross-validation removes each data location one at a time, predicts the associated data value, and compares the measured and predicted values. The statistics used in cross-validation serve as diagnostics to indicate whether the performance of the model is acceptable. Cross-validation prediction errors were used to guarantee that the prediction is unbiased, as close as possible to the measured value, and that the variability of the prediction is correctly assessed. The following cross-validation parameters were used for model performance evaluation: 1) The mean standardized (MS) prediction error was used to check if the model is unbiased—the closer the MS prediction error values to zero, the better the performance of the model. 2) The root-mean-square (RMS) prediction error was used to check whether the prediction was close to the measured values—the smaller the RMS prediction error, the closer the prediction is to the measured value. 3) The variability of the predicted data was assessed by evaluating the root-mean-square standardized (RMSS) prediction error value. If the value is close to 1, then the variability of the prediction is correctly assessed; if greater than 1 then it is underestimated; and otherwise it is overestimated. Table 13.5 shows that the MS values are close to 0 for all datasets, indicating that the model is unbiased. The RMS values of the different datasets are relatively small, which indicates a reasonable model prediction.

Table 13.5. Prediction errors of the different models

Dataset	MS	RMS	RMSS	ASE
Annual ET	0.01	2.29	0.73	3.47
Annual Precipitation	0.03	2.25	0.80	2.98
Seasonal ET	0.02	1.13	0.69	1.93
Seasonal Precipitation	0.02	0.95	0.89	1.09

Annual ET (in)

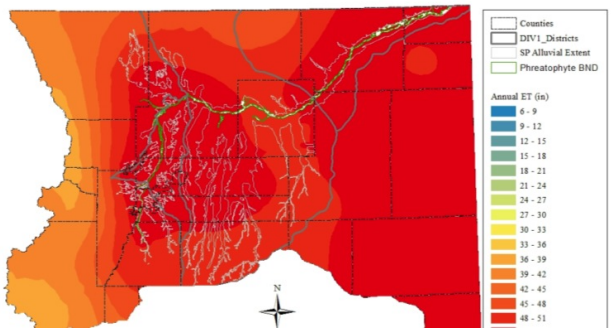

Annual Precipitation (in)

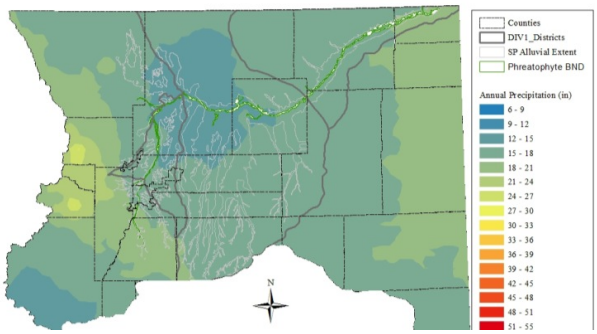

Seasonal ET (in)

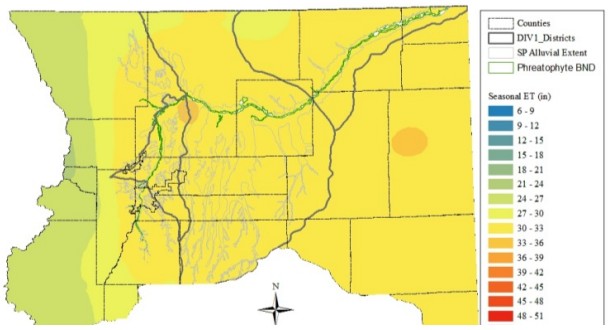

Seasonal Precipitation (in)

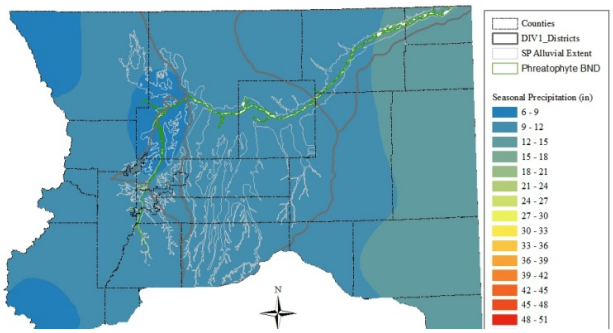

Figure 13.8. Developed maps for the annual and seasonal ET and precipitation data from 81 weather stations using the 30 year average (1981 - 2010) acquired from the National Climate Center Data (NCDC).

Figure 8 shows the developed maps for the annual and seasonal ET and precipitation data from 81 weather stations using the 30 year average (1981 - 2010) acquired from the National Climate Center Data (NCDC). The four maps' legends were standardized in order to visualize the relative colors of the maps. The semi-variogram of the previous figures was used with the ordinary kriging geostatistical model to generate the interpolated maps. Having 81 data stations allowed the use of geostatistical methods, which provided a means to study the spatial variability of the data (Pozdnyakova and Zhang, 1999). If a soil property is auto correlated in space, geostatistical methods, based on Matheron's regionalized variable theory (Matheron 1963), can be utilized to provide the best linear unbiased estimates (BLUE) of the variable of interest at

locations with no sample data. As mentioned by Deutsch and Journel, 1998, Kriging remains the best choice as a spatial estimation tool since it provides a single numerical value that is best in some local sense.

Using Weather Data With NDVI* to Develop ET_g

In practice, the estimation of the ET rate for a specific crop requires first calculating potential or reference ET and then applying the proper crop coefficients (K_c) to estimate actual crop evapotranspiration (ET_a). There is no K_c for phreatophytes; the standardized ET calculated from weather station data is used instead:

$$ET_i^* = \frac{(ET_i - P_i)}{(ET_{0-i} - P_i)} = \frac{(ET_g)}{(ET_{0-i} - P_i)}$$

For calibration of phreatophyte greenness (as NDVI*) to yield ET_g, peak greenness—i.e., NDVI*—was set equivalent to the peak ET rate. Appropriate for riparian vegetation, this peak ET rate can be estimated by a grass reference ET, ET_0.

Groeneveld et al. (2006) found that NDVI* and ET*, both dimensionless indices, were equivalent using data sets from three widely disparate western North American climates, locations, and phreatophyte species. NDVI* in this context functions as a crop coefficient mapped onto the ET_g distribution that is, itself, stretched from zero to one. To estimate phreatophyte vegetation:

NDVI*i=ET*i

TM data processed to NDVI* for each pixel in the riparian habitat provided a spatially correct estimate for ET*. ET* is a variable that can be decoded to provide estimated annual ET at any pixel "i" (ET_i) using raster values of annual total ET_o and precipitation for that pixel.

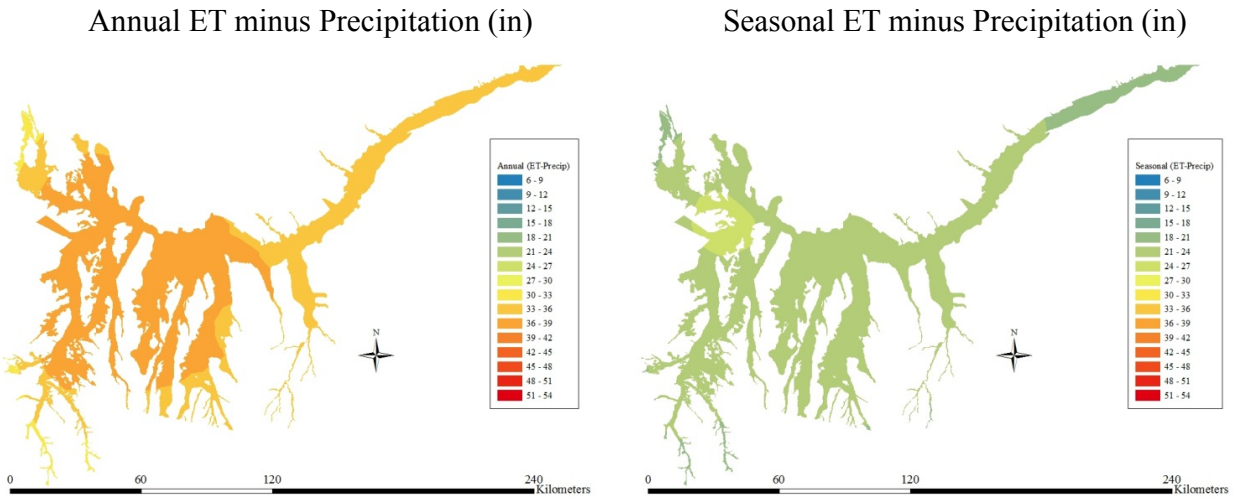

Figure 13.9. The developed annual and seasonal ET minus precipitation from weather station data.

Figure 13.9 shows both the annual and seasonal ET after subtracting precipitation in the form of 30 year averages that were developed from the weather data. The annual and seasonal ET maps were generated from the previous maps in Figure 13.8 by subtracting the precipitation raster from the ET raster. The generated rasters were also clipped over the alluvial extent of the South Platte in order to be able to zoom in and focus more on the phreatophyte details along the river. As is clear from the figure, the annual ET after subtracting precipitation is in the range between 2.00 and 3.50 ft, and the seasonal ET after subtracting precipitation is between 1.25 and 2.25. To generate the final ET, both the annual and seasonal ET (after subtracting the precipitation generated from the weather station data) are multiplied by the NDVI* generated from Landsat images for 2001. The three maps' legends were standardized in order to be able to visualize the relative colors of the maps. Figure 13.10 shows a flowchart that summarizes the

procedure of creating ET from Landsat 5 satellite images and weather data (reference ET and precipitation).

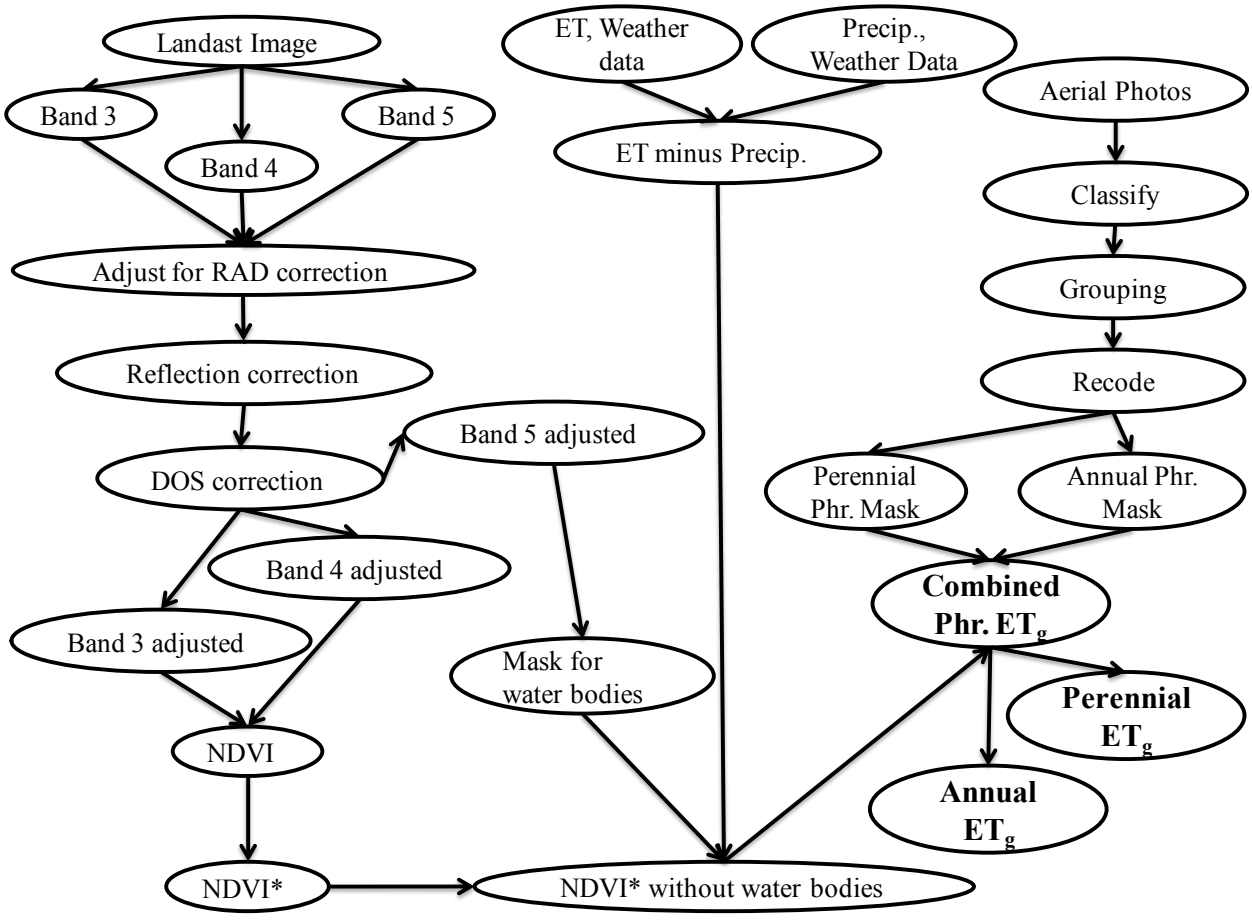

Figure 13.10. Flowchart summarizing the procedure for creating ET_g from Landsat 5 satellite images, weather data (reference ET and precipitation), and aerial photos.

Estimated phreatophyte ET

Figure 13.11 and

Table 13.6 show a flowchart comparison among the years 1990, 2001, and 2010 of the annual and seasonal phreatophyte ET (AcreFT). There is a clear trend of increasing phreatophytes from 1990 to 2010. However, this increase is different from slight to significant.

Table 13.6. Comparison among the years 1990, 2001, and 2010 of the annual and seasonal phreatophyte ET (AcreFT).

Reach #	1990		2001		2010	
	Annual ET (Acre FT)	Seasonal ET (Acre FT)	Annual ET (Acre FT)	Seasonal ET (Acre FT)	Annual ET (Acre FT)	Seasonal ET (Acre FT)
1	5246	3403	7479	4852	8230	5337
2	1081	686	1298	822	1555	985
3	2825	1750	3404	2109	4056	2513
4	4633	2897	5124	3203	6370	3986
5	4941	3137	5581	3542	7481	4749
6	2692	1697	3061	1929	4030	2540
7	19634	11947	22163	13481	24464	14876
8	9714	5861	11396	6876	15413	9301
9	6193	3726	6401	3851	6792	4087
10	11407	6808	11390	7110	13921	8317
11	13118	7903	13110	8890	20531	12363
12	26937	14297	23000	17000	34425	20612
13	7017	4192	7000	5577	9333	5577
Total	115,438	68303	120,406	79,242	156,601	95,241
Groeneveld 2007, Annual ET, 2001, was 123,686 when he used only 4 weather stations data						

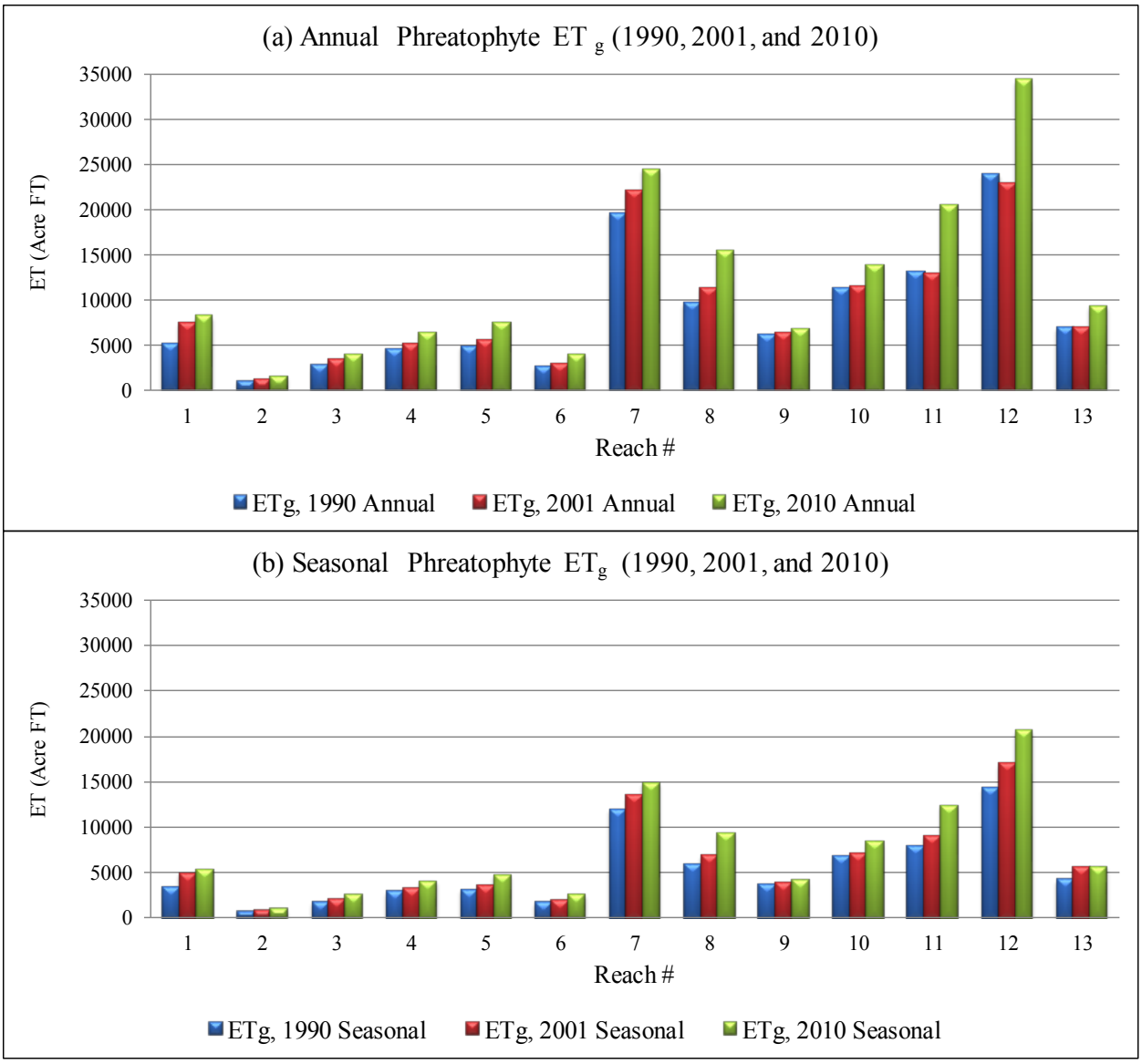

Figure 13.11. Comparison among the years 1990, 2010, and 2010 of the annual and seasonal phreatophyte ET (AcreFT).

Separate Annual from Perennial Phreatophytes

The separation of annual (trees) from perennial (grass or vegetation) phreatophytes is performed in two steps: 1) classify the images, and 2) apply grouping tool technique.

Classification

Classification is the process of sorting pixels into a finite number of individual classes based on their data values. If a pixel satisfies a certain set of criteria, then the pixel is assigned to the class that corresponds to that criteria set. There are two pixel classifications: supervised and unsupervised. Supervised classification is a method of generating signatures in which the analyst is directly involved in the pattern recognition process; i.e., selecting the training samples from the data that represent the patterns to be classified. Unsupervised classification uses an automated method for deriving the spectral categories and allows the user to specify guideline parameters. This method is based on the natural groupings of the data file values when they are plotted in spectral space. The statistics generated from the natural groupings are used to assign a class to each pixel according to its distance away from the mean. The unsupervised classification uses Iterative Self-Organizing Data (ISODATA), which repeatedly performs classifications and recalculates statistics by using a spectral distance formula.

Class Grouping Tools

The Class Grouping Tool (CGT) is used to label classes or clusters that have resulted from an unsupervised classification process. It incorporates automatic highlighting, improved class selection facilities, named groups and target classes, conflict detection, and a suite of Boolean tools to improve the labeling process. It supports two powerful cluster selection tools—the Dendrogram Tool and the Ancillary Data Tool. Figure 13.12 shows the dendrogram as a grouping tool technique. Classes that are spectrally similar to each other will frequently form tight spatial clusters when highlighted together in the CGT. The Dendrogram Tool provides a way of using spectral proximity to select classes within the CGT, where their spatial relationship

is readily viewable. This can be a powerful aid in making inferences about which classes should be grouped together, such as Deep Water (Lakes, Reservoirs). A dendrogram is a method of compressing an “n” by “n” matrix of spectral distances among classes into a readily-viewable hierarchical graphic. In the resulting dendrogram graph, classes that are spectrally similar are grouped together in the graph’s hierarchy. This hierarchy is created by finding the two classes (signature objects) that are nearest each other using the selected distance measure. These two classes are joined together into a new object. This procedure is continued until all of the signature objects are joined together.

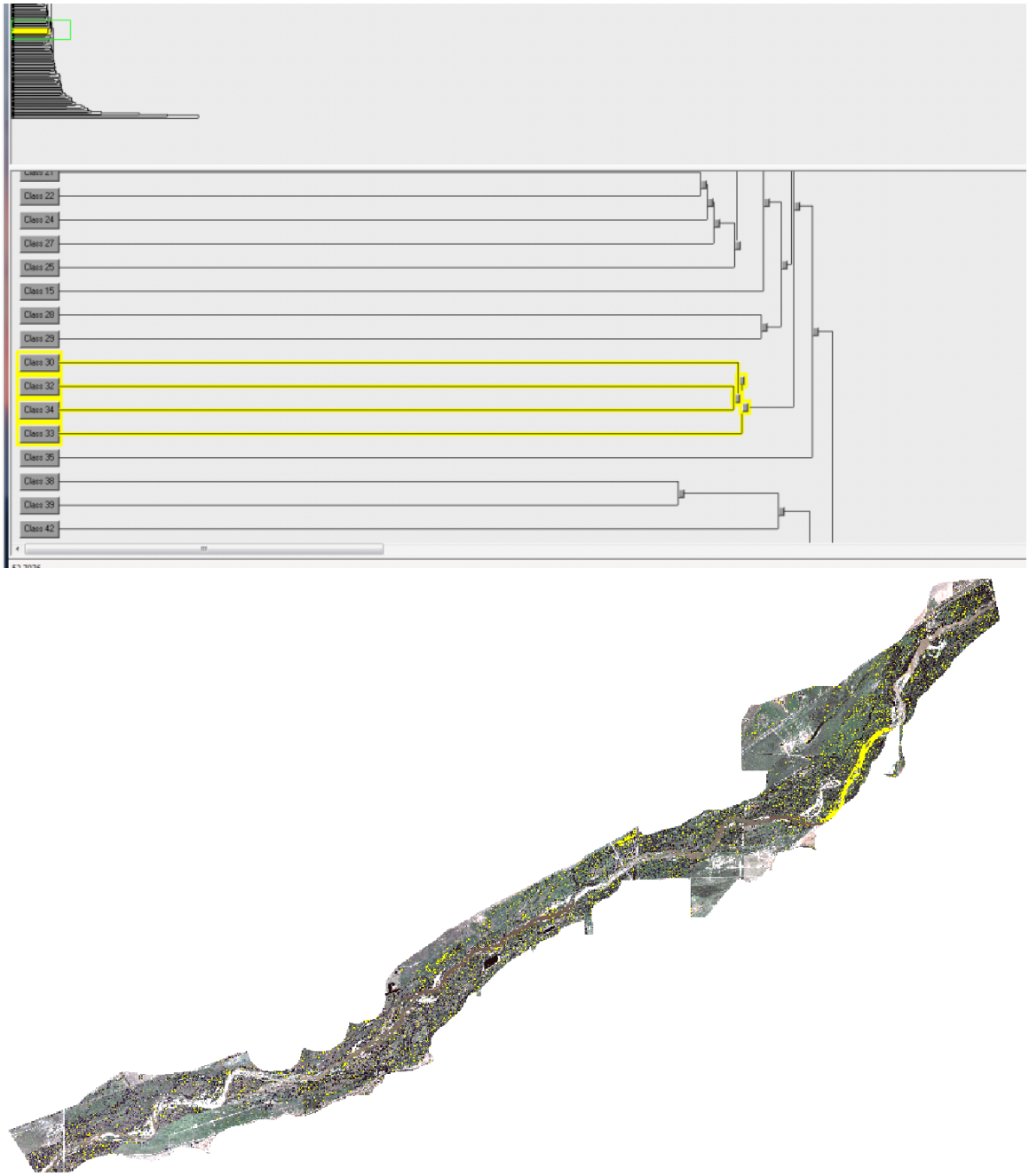

Figure 13.12. An example of using the dendrogram as a grouping tool technique.

Identifying and Resolving Similarities and Conflicts

The CGT allows any number of Class Groups representing each Target Class, and there is no limit on whether these groups overlap or conflict with each other. It is frequently the case

that a single class may properly belong with more than one target class. These classes are termed conflicted classes, and they generally create a speckle in the resulting final classification. Both Similarity and Conflict are measures of shared classes. Similar classes are shared by other groups within the same Target Class, while conflicted classes are shared by groups under a different Target Class.

Figure 13.13 shows an example of using the grouping tools technique to group similar classes in the unsupervised classified image. The unsupervised classified image is on the left side; the components of the grouping tools are on the right side. The classes are the individual clusters of pixels with similar spectral characteristics. These clusters are the result of unsupervised classification. The target classes are the final categories for interpreting. The class group is the saved groups of classes that represent a single target class. The working group is composed of the currently selected classes that are highlighted in the viewer. The target classes were set to the following: Annual Phreatophyte, Perennial Phreatophyte, Deep Water (Lakes or Reservoirs), Bare Soil, and Other, such as “Roads” or “None of the Previous Classes.” Cross-chairs or polygons can be used to specify the pixels of any specific class. Once selected, the class is automatically highlighted throughout the image. Figure 13.14 shows an enlarged portion of the image to show details, showing how grouping tools can distinguish between different classes, besides the area of the different classes can be quantified.

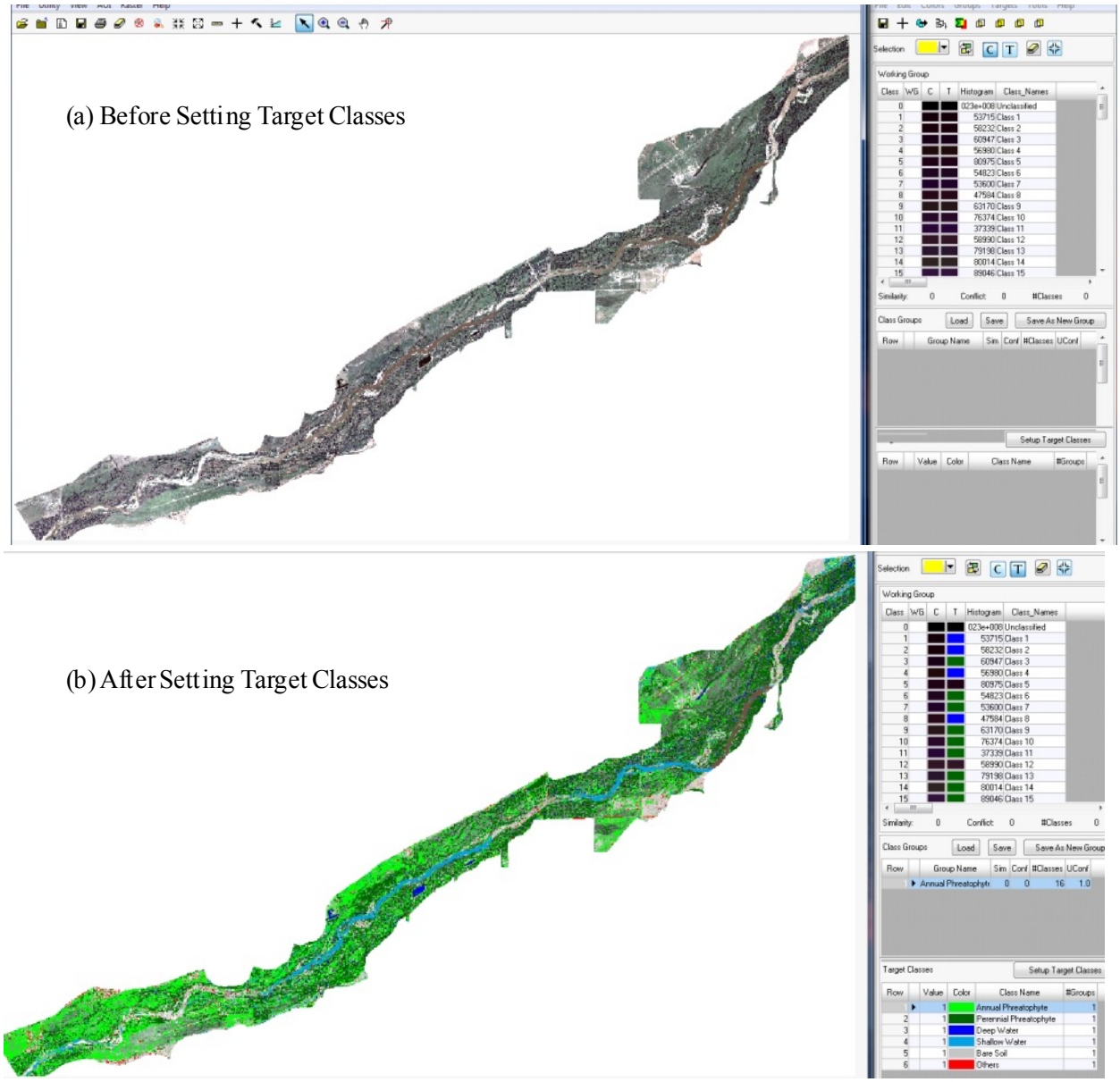

Figure 13.13. Applying grouping tool techniques: (a) before setting the target classes, (b) after setting the target classes.

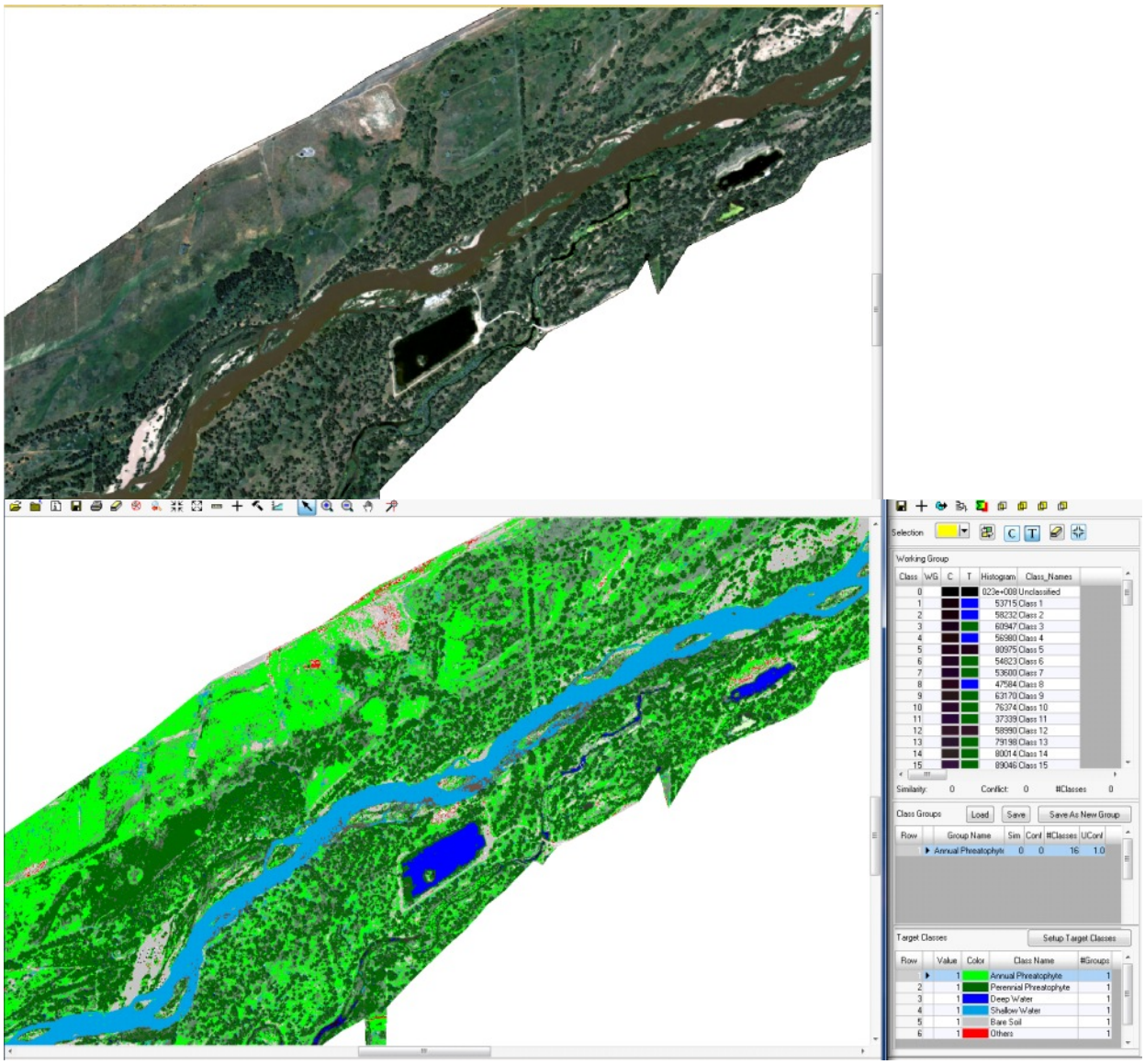

Figure 13.14. Applying grouping tool techniques.

Table 13.7. Comparison between the combined annual and seasonal phreatophyte ET_g (AcreFT) and the separated of the perennial from the annual for 2010.

	Combined Phreatophyte ET_g (AcreFT)		Separated Phreatophyte ET_g (AcreFT)	
Reach #	Annual	Seasonal	Perennial	Annual
1	8230	5337	763	2400
2	1555	985	320	661
3	4056	2513	1020	1700
4	6370	3986	2525	4834
5	7481	4749	1223	7090
6	4030	2540	1136	1652
7	24464	14876	1952	12284
8	15413	9301	674	7825
9	6792	4087	1315	2597
10	13921	8317	3200	4864
11	20531	12363	3555	7377
12	34425	20612	3998	12781
13	9333	5577	1942	6147
Total	156,601	95,241	23,622	72,211

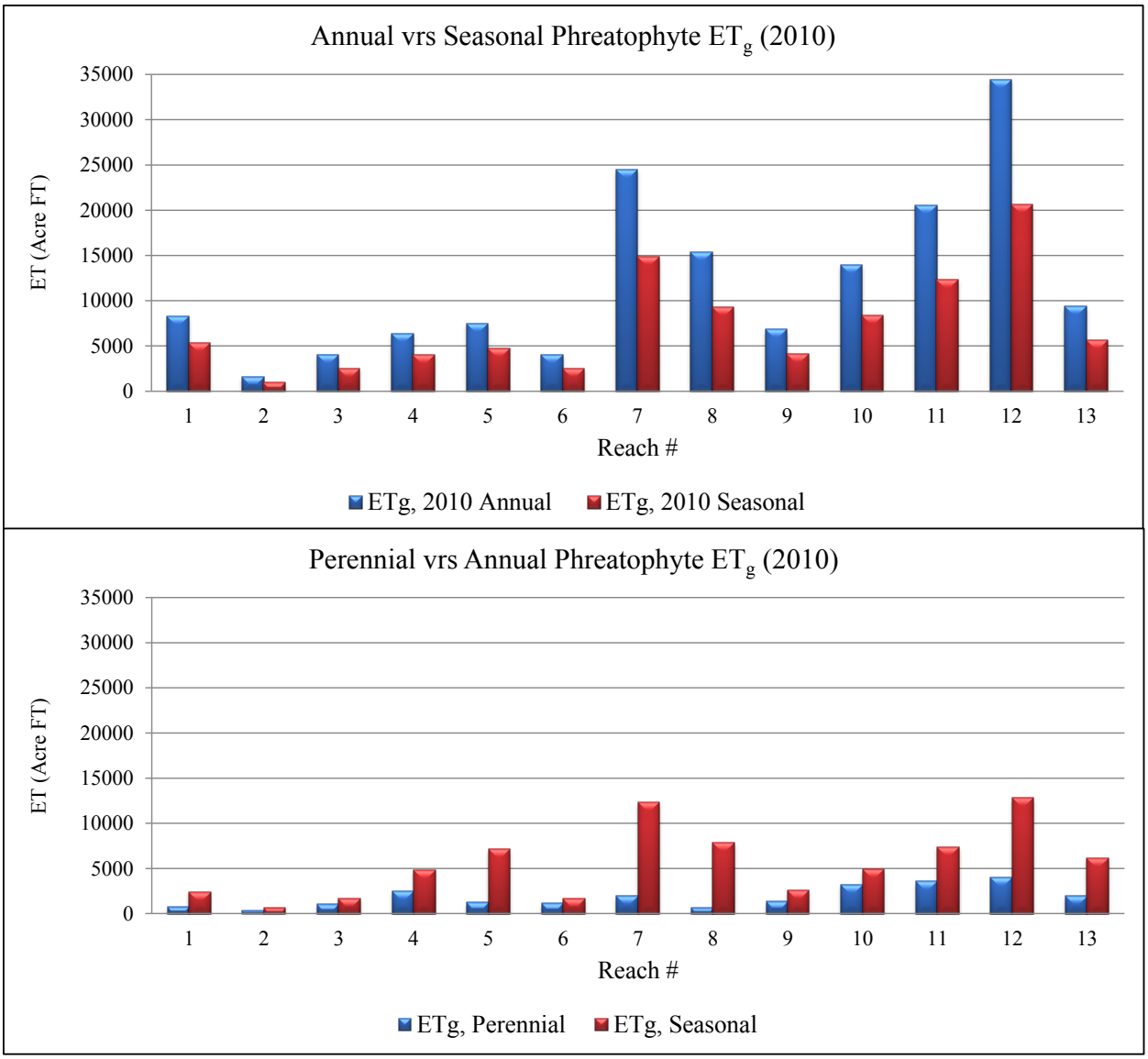

Figure 13.15. Comparison between the combined annual and seasonal phreatophyte ET_g (AcreFT) and the separated of the perennial from the annual for 2010.

Figure 13.15 as well as Table 13.7 show a comparison between the combined annual and seasonal phreatophyte ET_g (AcreFT) and the separated perennial and annual for 2010. The perennial and annual phreatophyte ET_g were developed using the aerial photos. The aerial photos of 1m*1m resolution were classified to be able to create individual classes of each object on the ground. After classification, the CGT was used to group classes of the same object. The resulting

raster was recoded twice. First, the perennial phreatophyte class was assigned to a value of 1 while the rest classes were assigned to a value of 0. The resulting raster masks everything except the perennial phreatophyte. Second, the annual phreatophyte class was assigned to a value of 1 and the rest of the classes were assigned to a value of 0. The resulting raster masks everything except the annual phreatophyte. It is clear that there is a significant reduction in the values of the phreatophyte ET_g when separating the perennial from the annual. This is mainly attributed to the following facts: 1) the areas of the perennial phreatophyte, mainly trees, are smaller than the areas of the seasonal phreatophyte; 2) to generate phreatophyte ET_g, the developed NDVI* is multiplied by the perennial mask of the aerial photos and the annual weather raster; 3) to generate the annual phreatophyte ET_g, the developed NDVI* is multiplied by the annual mask of the aerial photos and by the seasonal weather raster. The values of the seasonal weather raster are smaller than the values of the annual weather raster, which accounts for the significant reduction in the values of the resulting ET of the separated perennial and annual from the combined. In the mean time, to generate the combined phreatophytes ET_g, the developed NDVI* raster is multiplied by the developed annual weather raster. In fact, it is more reasonable to use seasonal weather data to generate the annual phreatophyte ET_g and the annual weather data to generate the perennial phreatophyte ET_g.

Conclusion

Phreatophytes are consuming a considerable amount from the groundwater that impacts the consumptive use and water budget of the South Platte. There is no crop coefficient that have been developed yet for the phreatophytes, which makes a challenge and opens this area for a lot

of investigations. One of the methods that have been used by the previous studies was to estimate the amount of vegetation of the phreatophyte by using some vegetation indices such as NDVI, then replace the crop coefficient with the standardized ET developed from the weather stations data. However, most of the previous studies were solely relied on the Landsat images, which have 30m*30m resolution, and a few weather stations data. The low resolution of the Landsat images does not allow for an accurate estimate of the phreatophytes. Also, the weather stations data are important because it plays an important role in estimating the ET. This study takes the advantages of the Landsat images in developing the NDVI and the advantages of the aerial photos that have high resolution. The high resolution of the aerial photos can lead to an accurate estimate as well as it can be used to separate the annual and the perennial phreatophytes. Using the aerial photos with the Lnadsat images allows us to use two approaches to estimate the phreatophyte ET_g, first is to use the NDVI* that was developed form Landsat 5 images with the annual weather data to estimate phreatophyte ET_g without separating the annual from perennial and second, to separate perennial and annual phreatophytes. The results of this study show that the phreatophytes in general increased from 1990 to 2010. The increase from 1990 to 2001 was slight for most of the reaches and there was a decrease in some reaches. However, there was an increase from 1990 to 2010 in all reaches. The perennial phreatophytes ET_g for the 2010 is less that the annual. The ET_g resulting from the separated annual and perennial phreatophytes is less than the phreatophytes ET_g when considered without separation.

References

Baugh, W.M., and Groeneveld, D.P. 2006. Broadband vegetation index performance evaluated for a low-cover environment. *International Journal of Remote Sensing.* Volume 27:4715-4730.

Chander, G., and Markham, B. L. Nov. 2003. Revised Landsat-5 TM radiometric calibration procedures, and post-calibration dynamic ranges. IEEE Trans. Geosci. Remote Sens., vol. 41, no. 11, pp. 2674–2677.

Chander, G., Markham,B. L, and Barsi, J. A. July 2007. Revised Landsat-5 Thematic Mapper Radiometric Calibration procedures. IEEE Trans. Geosci. Remote Sens., vol. 4, no. 3, pp. 490–494.

Chavez, P.S. Jr. 1988. An improved dark-object subtraction technique for atmospheric scattering correction of multispectral data. Remote Sensing of Environment, 24: 459-479.

Chong, D.L.S., Mougin, E., Gastellu-Etchegorry, J.P. 1993. Relating the global vegetation index to net primary productivity and actual evapotranspiration over Africa. International Journal of Remote Sensing 14, 1517–1546.

Harbaugh, A.W., Banta, E.R., Hill, M.C., McDonald, M.G., 2000. Modflow-2000, the U.S. Geological Survey modular groundwater model – user guide to modularization concepts and the ground-water flow process. US Geological Survey Open-File Report 00-92.

Ji, L. and Peters, A.J. 2003. Assessing vegetation response to drought in the northern Great Plains using vegetation and drought indices. Remote Sensing of Environment 87, 85–98.

Kerr, Y.H., Imbernon, J., Dedieu, G., Hautecoeur, O., Lagouarde, J.P., Seguin, B., 1989. NOAA AVHRR and its uses for rainfall and evapotranspiration monitoring. International Journal of Remote Sensing 10, 847–854.

Kustas, W.P., Perry, E.M., Doraiswamy, P.C., Moran, M.S. 1994. Using satellite remote sensing to extrapolate evapotranspiration estimates in time and space over a semiarid rangeland basin. Remote Sensing of Environment 49, 275–286.

Malo, A.R., Nicholson, S.E. 1990. A study of rainfall and vegetation dynamics in the African Sahel using normalized difference vegetation index. Journal of Arid Environments 19, 1–24.

McDonald, M.D., Harbaugh, A.W. 2003. The history of MODFLOW. Groundwater 41, 280–283.

Nichols, W.D. 2000. Regional ground-water evapotranspiration and ground-water budgets, Great Basin, Nevada. US Geological Survey Professional Paper 1628. 82pp.

Nichols, W.D., Laczniak, R.J., DeMeo, G.A., Rapp, T.R. 1997. Estimated ground-water discharge by evapotranspiration, Ash Meadows area, Nye County, Nevada, 1994: US Geological Survey Water Resources Investigation Report 97-4025, 13pp.

Seevers, P.M., Ottmann, R.W., 1994. Evapotranspiration estimation using a normalized difference vegetation index transformation of satellite data. Hydrological Sciences Journal 39, 333–345.

Szilagyi, J. 2002. Vegetation indices to aid areal evapotranspiration estimations. Journal of Hydrologic Engineering 7, 368–372.

Tucker, C.J., Nicholson, S.E. 1999. Variation in the size of the Sahara Desert from 1980 to 1997. Ambio 28, 587–591.

Wang, J., Rich, P.M., Price, K.P., 2003. Temporal response of NDVI to precipitation and temperature in the central Great Plains, USA. International Journal of Remote Sensing 24, 2345–3364.

Yang, L., Wylie, B.K., Tieszen, L.L., Reed, B.C., 1998. An analysis of relationships among climate forcing and time-integrated NDVI of grasslands over the US northern and central Great Plains. Remote Sensing of Environment 65, 25–37.

The ReSET (Remote Sensing of Evapotranspiration) model uses an energy balance algorithm to estimate evapotranspiration (ET) from a set of satellite images. The bureau of reclamation funded the development of the ReSET as an alternative to methods that use crop maps and crop coefficients to estimate water use. The main advantages of ReSET over the conventional crop coefficient method of estimating ET are: no need to map crop types and it can measure reduced ET from crops with a partial water supply.

Currently, Reclamation staff rely almost exclusively on the crop coefficient method to calculate consumptive water use by agriculture and riparian vegetation. Crops and riparian vegetation are mapped using remote sensing, and the results are placed in a Geographic Information System (GIS). Every vegetation type in the map is assigned a "crop coefficient," which estimates the proportion of water used by that vegetation type compared to a reference crop (usually grass or alfalfa) under the same weather conditions. Reference crop ET is predicted from local weather data using American Society of Civil Engineers (ASCE) standardized equations. Total water use for any crop for any time period is determined by multiplying the reference crop ET for that time period by the crop coefficient. Total water use is determined by multiplying the water use value for each crop type by the acreage of the crop.

The crop coefficient method is widely accepted, but has the unrealistic assumptions of: identical phenological development for all members of a given vegetation class and ideal growing conditions. The first assumption is never met due to variability in planting dates and natural variation in crop development, but many of the errors may be in different directions and, thus, cancel one another. Errors resulting from the assumption of ideal growing conditions are a more significant problem. Conditions such as reduced water supplies, pest and disease damage,

inadequate nutrients, salt buildup, or other such factors can reduce actual vegetation ET from the theoretical value.

The ReSET model uses an energy balance model to estimate ET.

R plus G plus H plus LE = 0

where:

R = net radiation flux at the surface

G = sensible heat flux to or from the ground

H = sensible heat flux to or from the atmosphere

LE = latent heat flux (ET)

ET is estimated as the residual of the energy balance equation after R, G, and H have been measured or estimated using satellite imagery and physical models. 24-hour estimates of ET generated from the satellite imagery are interpolated temporally using local weather station data to "fill in the gaps" between satellite overpasses. ReSET does not make the assumptions of uniformity and ideal growing conditions, and uses satellite imagery to solve the energy balance equation for every pixel in the image. The result is a continuously varying map of ET that offers more information to farmers and water managers than a similar product produced using crop coefficients.

XIII. Phreatophytes

b. Using Surface Energy Balance-Based Model to Estimate the Evapotranspiration of the Irrigated Crops and Phreatophytes of the South Platte River Basin

Using Surface Energy Balance-Based Model to Estimate the Evapotranspiration of the Irrigated Crops and Phreatophytes of the South Platte River Basin

Abstract:

Water resources management is important to secure agricultural production in order to face the daunting challenges from population growth with the existing limited resources of water. Evapotranspiration (*ET*) is the largest water user of the irrigation water and accuracy in *ET* estimation can be very valuable for better irrigation management, which can contribute to improving agricultural production and water conservation. Remote sensing has the potential to estimate *ET* and has the ability of capturing the spatial variability and it can provide regional estimates of *ET*. In this study, ReSET, a surface energy balance-based model, is used to estimate the *ET* of the irrigated crops and the phreatophtes of the South Platte River Basin. ReSET is based on surface energy balance and remote sensing and has ability to handle data from multiple weather stations. The objective of this study is to estimate the *ET* of all irrigated crops as well as phreatophtes of the South Platte. The study area is covered by three scenes with the following path/row (32/32, 33/32, and 33/33). All the available Landsat 5/7 images that has no clouds that can affect the study area were acquired and processed. Weather station data were collected from Northern Colorado Water Conservancy District (NCWCD), where the reference *ET* at the hour and at the day of each image acquisition date were considered as well as daily wend run. Digital elevation model (DEM) files were acquired for net radiation calculations of model. The results of this study show that the total *ET* for 2001 and 2010 are 1,955,712 and 1,905,240 AcreFT respectively with a slight decrease in 2010. Corn has the highest *ET* for both 2001 and 2010 with

38% and 39% of the total ET followed by alfalfa with 35% and 30% of the total ET. The rest of the crops represent from 25% to 30% of the total *ET*. Phreatophytes *ET* was separated from the *ET* of the irrigated crops and it has a total *ET* of 404,961 and 412,505 in 2001 and 2010 respectively with a slight increase in the year 2010.

Introduction:

The demand for water exceeds its availability in several of the world's large river basins. Irrigated agriculture is the largest consumer of water in river basins, and water savings upstream can lead to additional water developments downstream in the basin. Quantifying the consumption of water over large areas and within irrigated projects is important for water rights management, water resources planning, hydrologic water balances, and water regulation (Allen et al. 2007 b). Traditionally, *ET* from agricultural fields has been estimated by multiplying a weather-based reference *ET* by a crop coefficient (*Kc*) determined according to the crop type and growth stage. However, there is typically some questions as to whether actual vegetative and growing conditions compare with the conditions represented by the idealized *Kc* values, especially in water short areas. In addition, it is difficult to predict the correct crop growth stage dates for large populations of crops and fields (Allen et al. 2007 b). In the meantime, most conventional methods in estimating *ET* are based on point measurements that limit their ability to capture the spatial variability in a study area. *ET* varies spatially and seasonally according to weather and vegetation cover conditions (Hanson 1991). Hydrological models and remote sensing techniques are advanced tools that are better suited to estimate the evaporation and the related hydrological processes at the regional scale (Beven et al., 1988). The advantage of the hydrological models have an advantage in simulating the effects of man-induced scenarios on

regional hydrology. However, the disadvantage is that considerable expertise in model use and extensive field data are required to make proper model simulations and the implementation can take several man-years. The major advantage of applying remote sensing based evaporation procedures is that the water consumed by the soil–water–vegetation system can be derived directly without the need to quantify other complex hydrological processes. The relationship between the water released from the head regulator for irrigation and water consumption can be determined without the need to explicitly address how water flows and is recycled in an irrigation scheme or river basin (Bastiaanssen 2000).

Remote sensing data provided by satellites are a means of obtaining consistent and frequent observation of spectral reflectance and emittance of radiation of the land surface on micro to macro scale (Bastiaanssen et al. 1998 a). Remote sensing has several advantages over the traditional methods in estimating ET. It has the ability of capturing the spatial variability and it can provide regional estimates of *ET* at low cost. *ET* models based on surface energy balance (SEB) and remote sensing data estimate *ET* with a high level of spatial resolution. SEB algorithms are based on the rationale that *ET* represents a change in the state of water, from liquid to gas, by a process that requires available energy (*ET* = net radiation — heat to the soil — heat to the air) in the environment for the vaporization of water (Su et al. 2005). There are several SEB models in the literature (Gowda et al. 2008) which mainly differ in the way how sensible heat flux (*H*) is calculated. SEB algorithm for land (SEBAL) (Bastiaanssen et al. 1998a) uses hot and cold pixels within each satellite image to develop an empirical temperature difference equation, however, SEB index (Menenti and Choudhury 1993) is based on the contrast between wet and dry areas.

Elhaddad and Garcia (2008) proposed a methodology to incorporate multiple weather stations into a SEB model called remote sensing of *ET* (ReSET) in order to address the variable weather conditions per location encountered by the remote sensing platform's coverage area at the time of overpass. The use of single weather stations does not accurately represent weather conditions such as those created by topographic and/or microclimatic conditions within the coverage of a satellite scene. ReSET is a SEB model built on the same theoretical basis of its two predecessors: mapping evapotranspiration at high resolution with internalized calibration (METRIC) (Allen et al. 2007a, b) and surface energy balance algorithm for land (SEBAL) (Bastiaanssen et al. 1998 a, b). ReSET can be used in both the calibrated and the uncalibrated modes. The calibrated mode is similar to METRIC in which the reference *ET* from weather stations is used to set the maximum *ET* value in the processed area, while in the uncalibrated mode, the model follows a similar procedure as SEBAL where no maximum *ET* value is imposed. ReSET has additional ability to handle data from multiple weather stations.

Method

This section describes the development of a surface energy balance-based model ReSET for estimating actual crop *ET*. ReSET is an enhanced *ET* estimation model based on the methodology implemented in the surface energy balance algorithm for land (SEBAL) (Bastiaanssen *ET* al. 1998a, b). SEBAL allows the user to arrive at *ET* estimates using data from only one weather station. ReSET expands upon SEBAL and takes into consideration the spatial variability in weather parameters over a region by using data from multiple weather stations. ReSET represents an improved method for looking at *ET* at a larger scale, such as a region or river basin scale. ReSET model is applied in this research to estimate *ET* using several Landsat

5/7 scenes. *ET* is computed for each pixel in the satellite image for the instantaneous time and the day of the image. The process is based on a complete energy balance for each pixel where *ET* is predicted from the residual amount of energy remaining from the classical energy balance: *ET* = net radiation — heat to the soil — heat to the air. Landsat imagery contains visible bands (1, 2, 3), infrared bands (4, 5, 7), and a thermal infrared band (6). From the visible and infrared bands, surface albedo is derived. The normalized difference vegetation index (NDVI) is derived from bands 3 and 4, and the surface temperature is derived from the thermal infrared band (band 6). These three components are combined with the digital elevation models (DEM) and surface roughness to calculate the net radiation (*Rn*) based on a function developed by Bastiaanssen (2000). The soil heat flux (*G*) is calculated empirically using albedo, NDVI, surface temperature, and sensible heat flux. The model's algorithm computes most of the essential hydro meteorological parameters empirically from the satellite images. In the model, the surface energy balance components, the sensible heat flux *H*, is solved iteratively, and the *ET* is derived as the closure term of the surface energy balance equation:

$$LE = (R_n - G) - H \tag{1}$$

where R_n = net radiant energy exchange at the earth's surface, which is called net radiation; LE = evapotranspiration expressed as latent heat flux density; H = net surface-atmosphere flux of sensible heat; and G = soil heat flux density.

The approach implemented in ReSET to estimate the latent heat flux (*LE*) that yields the instantaneous evapotranspiration relies on selecting two locations in the study region. The first location is called the wet pixel. Water vapor at this location is assumed to be released based on the atmospheric requirement; thus, the vertical difference in temperature is down to the minimum. Under such conditions, the sensible heat flux (*H*) goes to zero and components of the

surface energy balance equation are reduced to net radiation *Rn* and soil heat flux *G* and latent heat flux *LE*:

$$LE = (R_n - G) - 0 \quad (2)$$

The wet pixel represents one of the two extreme pixels used to solve the energy equation. The second extreme pixel is the dry pixel at which *ET* is assumed to be zero, meaning that the latent heat flux is assumed to be zero (*LE* = 0). This assumption makes it possible to estimate the sensible heat flux (H) at this location since it is equal to

$$H = R_n - G \quad (3)$$

For a wet pixel, the difference in temperature between the near surface and the air (*dt*) can be assumed to be zero since maximum evaporation conditions are assumed to exist. For a dry pixel, *dt* is calculated for an air temperature of 20°C. Using the assumption that *dt* at a wet pixel equals zero (i.e., *H* wet = 0), the value of *H* at a dry pixel can be calculated. Once the values of *H* are known at two extreme pixels (wet and dry), *H* can be calculated for the rest of the image.

The first calculation of *H* is a preliminary estimate, and calculations for *H* must be repeated until *H* reaches stability. The instability is caused by the fact that air has three stability conditions (stable, unstable, and neutral). Stability conditions must be taken into consideration during the calculation of *H* since they affect the aerodynamic resistance to heat transport that directly affects the value of sensible heat flux (*H*). Once *H* reaches stability, the latent heat flux can be calculated using the energy balance equation Eq. (1). The latent heat flux is then converted to estimate the instantaneous evapotranspiration. Assuming that the instantaneous evapotranspiration fraction is constant over a whole day (24 h), the instantaneous and day evapotranspiration can be calculated as follows:

$$ET_{inst-fraction} = LE/(R_n - G) \quad (4)$$

where: *Rn*, *G*, and *LE* are all instantaneous, then the *ET* (24-h) is calculated by:

$$ET_{24} = 86{,}400 * ET_{inst-fraction} * (R_{n24} - G_{24}) / L \quad (5)$$

where: ET_{24}= 24-h evapotranspiration; 86,400=time conversion from seconds to days; R_{n24}= 24-h net radiation; G_{24}= 2 4-h soil heat flux; *L* = latent heat of vaporization that is used to convert the energy to mm of evaporation. *L* is based on the surface temperature and represents the energy needed to evaporate a unit mass of water as calculated by the following equation developed by Harrison (1963):

$$L = (2.501 - 0.00236 * (T_S - 273.16)) * 10^6 \quad (6)$$

where T_S = surface temperature in Kelvin.

To estimate the value of *H* for the rest of the image pixels, the Monin-Obukhov length similarity theory is used for correcting the calculations of sensible heat flux for atmospheric stability conditions. This is achieved through an iterative process where the surface aerodynamic resistance of heat transport (r_{ah}, s m^{-1}) at the cold and hot pixels are updated after each iteration until numerical stability is reached for the aerodynamic resistance (typically less than 5% difference between consecutive iterations of r_{ah}). Once numerical stability is reached, then *H* is calculated for the entire image using the coefficients of the *dT* function and the "r_{ah}" updated values. Next the spatially distributed latent heat flux is calculated using the energy balance equation Eq.(1). Using the estimated *LE* grid, the instantaneous "actual" *ET* grid (ET_{inst}, mm h^{-1}) and the evaporative fraction grid are calculated. For the model in the uncalibrated mode the 24-h *ET* (full day) is calculated by assuming that the instantaneous evaporative fraction, calculated at the time of the satellite overpass, is constant over a whole day (24 h). More details on the procedure of how *ET* can be estimated from satellite imagery is presented in Bastiaanssen et al.

(1998b), Bastiaanssen (2000), Bastiaanssen et al. (2002), Allen et al. (2005), and Tasumi et al. (2005).

Acquiring Landsat 5/7 images:

The study area is covered by three scenes of the following path/row (32/32, 33/32, and 33/33). All the Landsat 5/7 images of the 2001 and 2010 seasons that cover the whole season and do not have clouds that affect the study area were acquired. Clouds affect the calculations of *ET* when using remote sensing. Even a thin layer of clouds will produce an error in the calculations, since the areas covered by clouds will reflect as cool areas, which would be misclassified as actively growing areas with high *ET* values. Therefore, the used Landsat scenes was selected in a way that cloud cover does not affect the study area. In case where a small areas of the scene has cloud cover, a cloud mask was created to eliminate those areas that were covered by clouds or cloud shadows. Due to a problem with the Landsat 7, which referred to as the Scan Line Corrector Anomaly. On May 31st, 2003 Landsat 7's scan line corrector failed that causes strips on the images. Therefore, for the year 2001, both Landsat 5 and 7 were acquired since there are no strips at Landsat 7 while for the year 2010, only Landsat 5 images were acquired because of the strips in Landsat 7 that affect the study area. Each image was processed separately to generate *ET* raster for the day of the image acquisition date. Once, all the images for a specific season were processed, and then they are interpolated to generate an accumulated raster for the ET of the whole season. To generate the accumulated image, the start date and the end date of the interpolation was set to be May 1st and September 30th. After completing this process for all images of the three scenes, they are mosaicked to generate one raster for the whole season for

study are. Table 13.8 shows all the landsat 5/7 images used in this study to develop ET of the irigagated crops and phreatophytes of the South Platte River Basin.

Table 13.8. Landsat 5/7 scenes ID and acquisition dates.

Scene ID	Acquisition Date	Scene ID	Acquisition Date
lt50320322001117xxx02	27-Apr-01	le70330322001116edc00	26-Apr-01
le70320322001157edc00	6-Jun-01	le70330322001132edc00	12-May-01
lt50320322001181xxx01	30-Jun-01	lt50330322001156xxx02	5-Jun-01
lt50320322001197lgs01	16-Jul-01	lt50330322001188lgs02	7-Jul-01
lt50320322001229lgs01	17-Aug-01	lt50330322001220lgs01	8-Aug-01
lt50320322001245lgs01	2-Sep-01	lt50330322001236lgs01	24-Aug-01
le70320322001253edc00	10-Sep-01	le70330322001276edc00	1-Sep-01
le70320322001269edc00	26-Sep-01	lt50330322001252lgs01	9-Sep-01
lt50320322001309lgs01	5-Nov-01	le70330322001308edc00	4-Nov-01
le70330332001132edc00	12-May-01	LT50320322010094PAC01	4-Apr-10
lt50330332001140xxx02	20-May-01	LT50320322010126PAC01	6-May-10
lt50330332001188lgs02	7-Jul-01	LT50320322010142PAC01	22-May-10
le70330332001196edc00	15-Jul-01	LT50320322010174EDC00	23-Jun-10
lt50330332001220lgs01	8-Aug-01	LT50320322010190PAC01	9-Jul-10
lt50330332001236lgs01	24-Aug-01	LT50320322010222PAC01	10-Aug-10
le70330332001244edc00	1-Sep-01	LT50320322010238PAC01	26-Aug-10
lt50330332001252lgs01	9-Sep-01	LT50320322010254EDC00	11-Sep-10
lt50330332001268lgs01	25-Sep-01	LT50320322010270EDC00	27-Sep-10
le70330332001276edc00	3-Oct-01	LT50320322010286EDC00	13-Oct-10
LT50330322010117PAC01	27-Apr-10	LT50330332010149PAC02	29-May-10
LT50330322010149PAC02	29-May-10	LT50330332010181EDC00	30-Jun-10
LT50330322010181EDC00	30-Jun-10	LT50330332010197EDC00	16-Jul-10
LT50330322010197EDC00	16-Jul-10	LT50330332010229PAC01	17-Aug-10
LT50330322010213PAC01	1-Aug-10	LT50330332010245EDC00	2-Sep-10
LT50330322010229PAC01	17-Aug-10	LT50330332010261EDC00	18-Sep-10
LT50330322010245EDC00	2-Sep-10	LT50330332010277EDC00	4-Oct-10
LT50330322010277EDC00	4-Oct-10		

Digital Elevation Model (DEM) Data:

Digital elevation model (DEM) files were acquired and processed for the whole study area. The DEM is important because it is used for net radiation calculations of the ReSET model. Files were downloaded in sdts format and transformed to DEM format, then to raster format. Raster files were then mosaicked for the whole area of the study area. Figure 13.16 shows the DEM of the study area as well as the weather stations locations. The figure shows how the elevation can affect the weather station data. For the weather station at the far West, the elevation is 1725 meter, while for the weather station at the far West, the elevation is 1140 meter, with a difference of about 500 meters between the two stations. This reflects the importance of considering several weather stations in the calculation of the ReSET model.

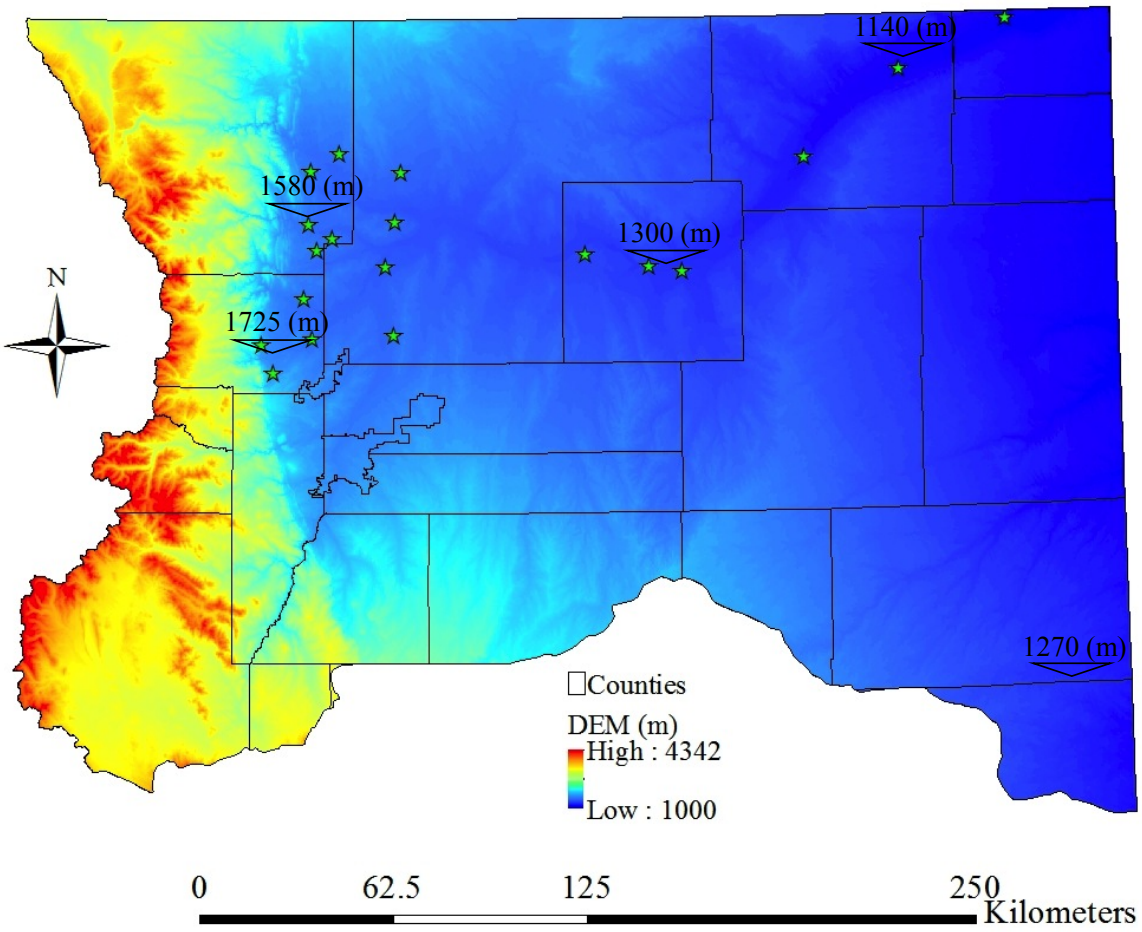

Figure 13.16. Digital Elevation Model (DEM) of the study area.

Irrigated Parcels:

The irrigated crops and phreatophytes of the years 2001 and 2010 were obtained from the South Platte Decision Support System (SPDSS). Figure 13.17 shows the shapefile of the irrigated parcels and the phreatophytes at the South Platte River Basin.

Table 13.9 show the areas of the different crops as well as phreatophytes. The dominant crops in both years are alfalfa, corn, and grass pasture. However, dry beans, small grains, sugar beets, and wheat are grown in significant amounts, but fluctuate for year to another. As an example, there are 1,660 wheat parcels in 2010, while in 2001; there are no single parcel of wheat. Also, there are 1,977 parcels of small grains in 2001 while in 2010 only 15 parcels. The total number of irrigated parcels in 2001 is 27,391 with a total area of 910,518 acres while in 2010 the total number of irrigated parcels is 24,950 with a total are of 850,546 acres. The total area of the phreatophytes is 201, 632 acres in 2001 and 2010. The irrigated parcels and the phreatophytes are using their consumption water from surface water, groundwater, or both.

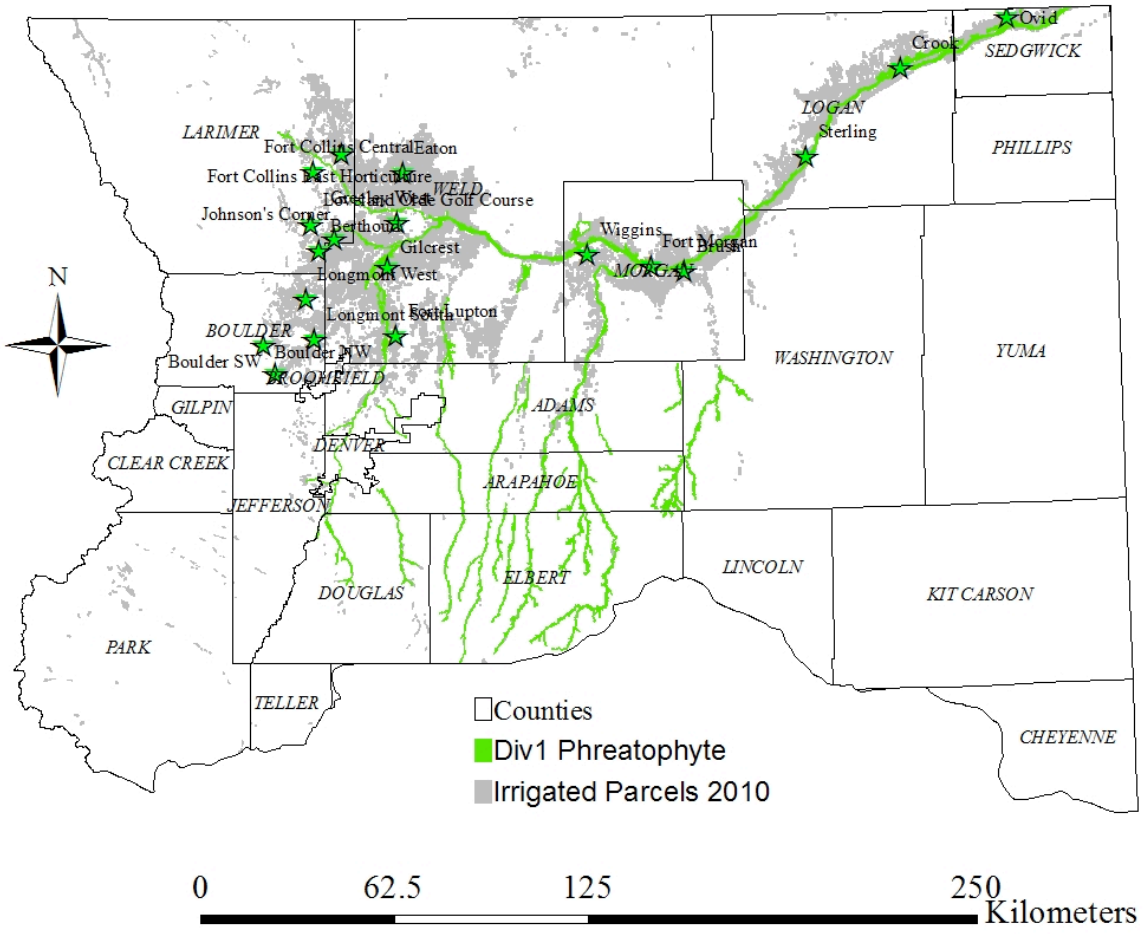

Figure 13.17. Irrigated Parcels of 2010 and phreatophyte shapefiles.

Weather Station Data:

Weather station data were collected from Northern Colorado Water Conservancy District (NCWCD) for the years 2001 and 2010. Data from twenty-one weather station were considered for generating *ET* using ReSET model. Reference *ET* at the hour and the day of each image acquisition date was considered as well as daily wend run. After generating *ET* for each image, the daily reference *ET* and wind run for each day of the season were considered *ET* ratser for each day of the season, then all the rasters are interpolated to generate an accumulated *ET* raster for the whole season. For interpolating the developed raster of each image to generate the seasonal *ET*. Figure 13.18 shows three examples of the daily wing run, the instantaneous, and the daily reference *ET* grid of the weather stations on august 26, 2010. The figure shows how wind run goes from 30 mph at the far west to 200 mph at the Far East. This reflects the importance of including several weather stations as well as including the DEM files since both of them can affect the calculation of the ReSET model.

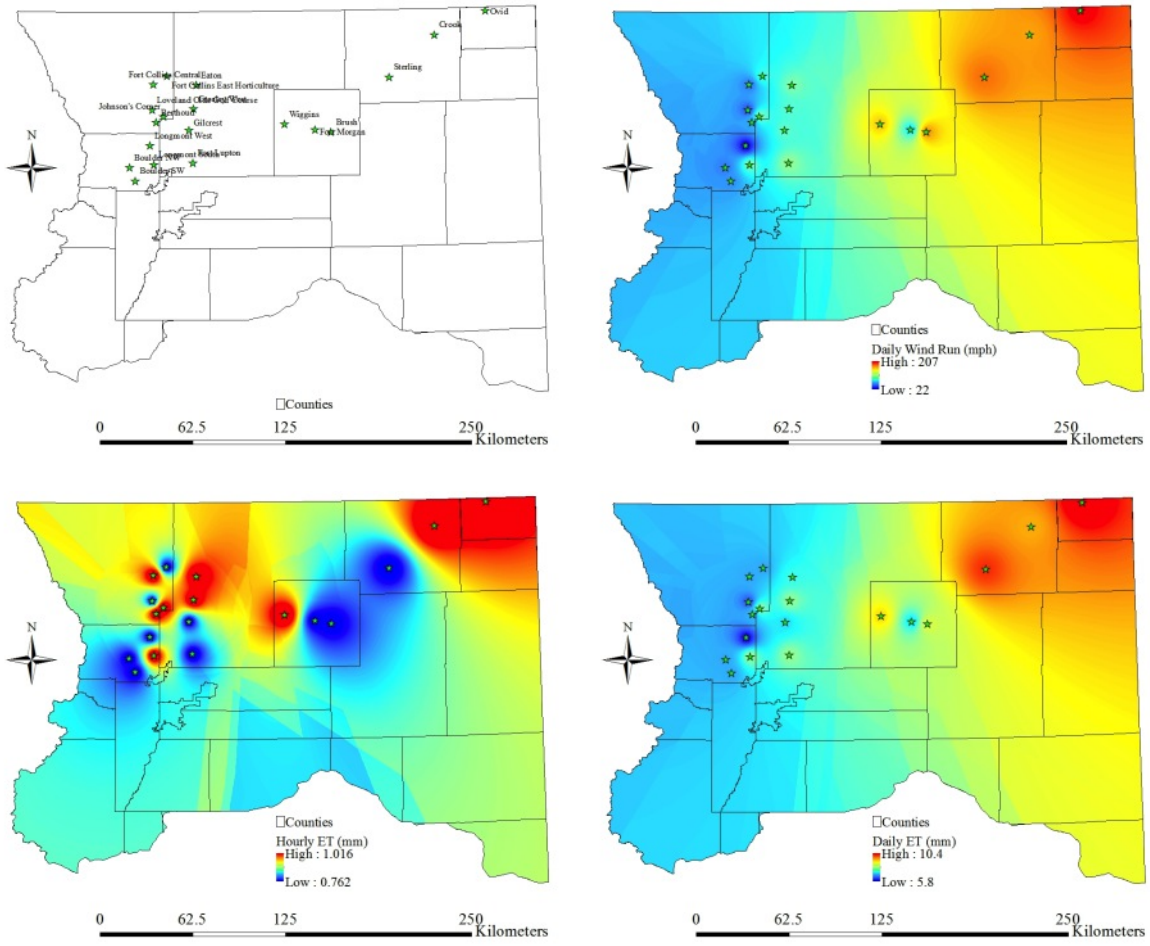

Figure 13.18. Weather stations, hourly *ET* (mm), and daily *ET* (mm) developed from weather stations.

Table 13.9. Areas of different crops and phreatophytes of 2001 and 2010

	2001			2010		
Crop	# of irrigated parcels	Area (acre)	% of Total	# of Irrigated Parcels	Area (acre)	% of Total
Alfalfa	10,722	310,521	27.92%	7,215	240,049	21.58%
Barley	NA	NA	NA	280	8,472	0.76%
Blue Grass	NA	NA	NA	40	2,170	0.20%
Corn	7,471	333,943	30.03%	8,068	328,562	29.54%
Dry Bans	1,006	29,401	2.64%	91	4,775	0.43%
Grass Pasture	4,535	120,073	10.80%	6,829	182,600	16.42%
Orchard	83	2,239	0.20%	2	20	0.00%
Small Grains	1,977	65,849	5.92%	15	405	0.04%
Snap Beans	NA	NA	NA	5	291	0.03%
Sod Farm	114	5,246	0.47%	1	35	0.00%
Sorghum	NA	NA	NA	7	70	0.01%
Sugar Beets	756	26,904	2.42%	584	23,546	2.12%
Sunflower	NA	NA	NA	67	2,639	0.24%
vegetables	727	16,343	1.47%	86	2,625	0.24%
Wheat	NA	NA	NA	1,660	54,286	4.88%
Total	27,391	910,518	100.00%	24,950	850,546	100.100%
Phreatophyte		201,632	18.13%		201,632	19.16%

Methodology

Selecting Cold and Hot Points:

The approach implemented in ReSET to estimate the latent heat flux (*LE*) that yields the instantaneous evapotranspiration relies on selecting two locations in the study region. The first location is called the wet pixel. Water vapor at this location is assumed to be released based on the atmospheric requirement; thus, the vertical difference in temperature is down to the minimum. Under such conditions, the sensible heat flux (*H*) goes to zero and components of the surface energy balance equation are reduced to net radiation R_n and soil heat flux *G* and latent heat flux *LE*. The wet pixel represents one of the two extreme pixels used to solve the energy equation. The second extreme pixel is the dry pixel at which *ET* is assumed to be zero, meaning that the latent heat flux is assumed to be zero ($LE = 0$). This assumption makes it possible to estimate the sensible heat flux (*H*) at this location. For a wet pixel, the difference in temperature

between the near surface and the air (*dt*) can be assumed to be zero since maximum evaporation conditions are assumed to exist. The basic assumption to obtain the value of *H* for each pixel in the image is that the air temperature gradient between near the ground surface and/or within the canopy and the adjacent screen level air layer changes linearly (i.e., is proportional) with the ground surface temperature [T_s (*K*)]. This is defined by a linear model represented by a "*dT*" function (i.e., $dT = aTs + b$), Bastiaanssen et *al*. (1998a). Models that use reference *ET* as a calibration method place some conditions on the selection of the cold pixel. Allen et al. (2005) recommend the cold pixel be close to the weather station (20 to 30 km) in METRIC model calibration. They also recommend the image should be split into several subareas and each subarea should be processed with its own hot and cold pixels when significant variation in weather conditions exist. This solution provides better estimates for *ET* than use of one reference cold and hot pixel for the whole image. Figure 13.19 shows an example selecting the model for cold and hot poins. The model select these points on a search radious of 10 kilometers for the closest weather station. The selection of cold points should be in a well irrigated filed and the selection of hot points sould be in a fallow field. Figure 13.19 show the hot and cold points with the surface temperature raster as a background on the left and with the original landsat 5 image as backgorund on the right.

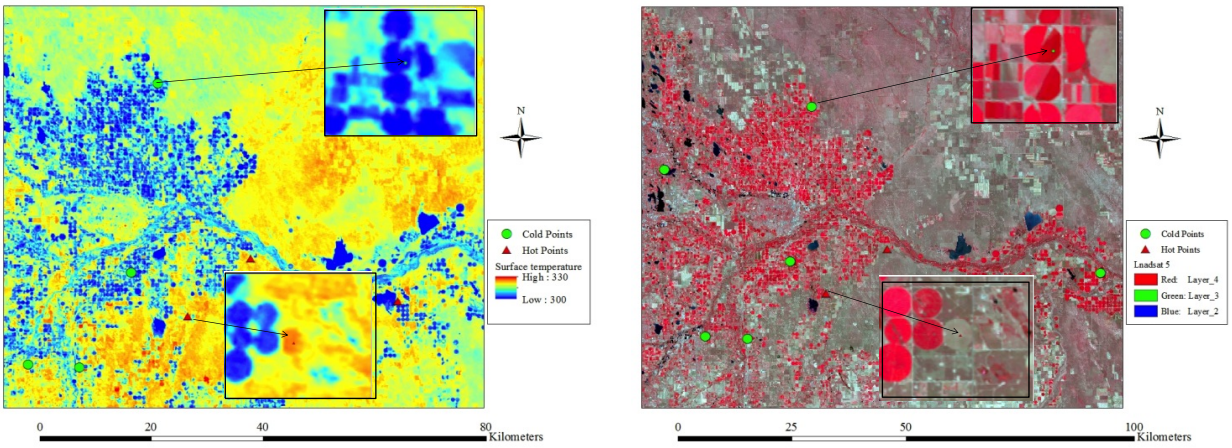

Figure 13.19. Examples of cold and hot points displayed on surface temperature raster on the left and on the original landsat 5 image.

Generating *ET* Using ReSET Model and Landsat Images:

The ReSET model is applied in this article to estimate *ET* using several Landsat 5 scenes. *ET* is computed for each pixel (the size of the pixel depends on the type of satellite image) in the satellite image for the instantaneous time of the image. The process is based on a complete energy balance for each pixel where *ET* is predicted from the residual amount of energy remaining from the classical energy balance. The algorithm used to calculate the components of the surface energy equation from Landsat imagery can be summarized as follows: Landsat imagery contains visible bands (1, 2, 3), infrared bands (4, 5, 7), and a thermal infrared band (6). From the visible and infrared bands, surface albedo is derived. The normalized difference vegetation index (NDVI) is derived from bands 3 and 4, and the surface temperature is derived from the thermal infrared band (band 6). These three components are combined with the digital elevation models (DEM) and surface roughness to calculate the net radiation (R_n) based on a function developed by Bastiaanssen (2000). The soil heat flux (G) is calculated empirically using albedo, NDVI, surface temperature, and sensible heat flux. Clouds affect the calculations of *ET*

when using remote sensing. Even a thin layer of clouds will produce an error in the calculations, since the areas covered by clouds will reflect as cool areas, which would be misclassified as actively growing areas with high *ET* values. The cloud cover in the seven Landsat scenes used ranged from 0 to 14%. A cloud mask was created for each image to eliminate those areas of the images that were covered by clouds or cloud shadows. Figure 13.20 shows an example of ReSET model output: (a) individual *ET* raster generated from single image, (b) interpolation of *ET* rasters of the whole season, (c) the final *ET* raster of the whole season from one scene.

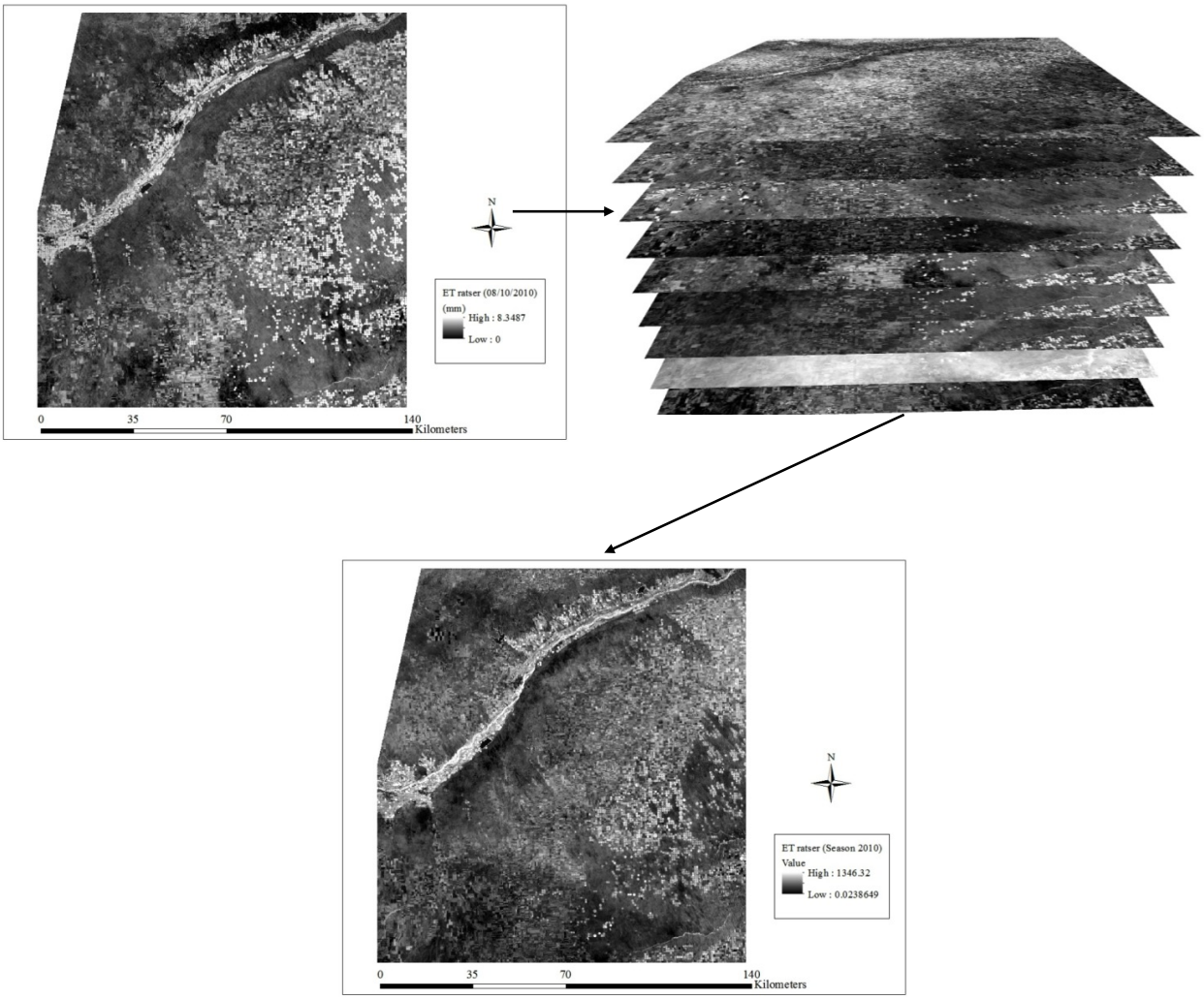

Figure 13.20. Example of ReSET model output: (a) individual *ET* raster generated from single image, (b) interpolation of *ET* rasters of the whole season, (c) the final *ET* raster of the whole season from one scene.

ET AcreFT of Irrigated Crops and Phreatophytes:

Figure 13.21 as well as

Table 13.10 show the areas and *ET* of each individual irrigated crop as well as the phreatophyte of the South Platte River Basin.

Table 13.10 shows all the crops as well as the phreatophytes, however, the pie charts shows the dominant crops and crops with an area of less than 5% of the total area, they were combined together and mentioned as others in order to make the comparison easy. The total *ET* for 2001 and 2010 are 1,955,712 and 1,905,240 AcreFt respectively with a slight decrease in 2010. Corn has the highest *ET* for both 2001 and 2010 with

38% and 39% of the total ET followed by alfalfa with 35% and 30% of the total ET. The rest of the crops represent from 25% to 30% of the total *ET*. Phreatophytes *ET* was separated from the *ET* of the irrigated crops and it has a total *ET* of 404,961 and 412,505 in 2001 and 2010 respectively with a slight increase in the year 2010.

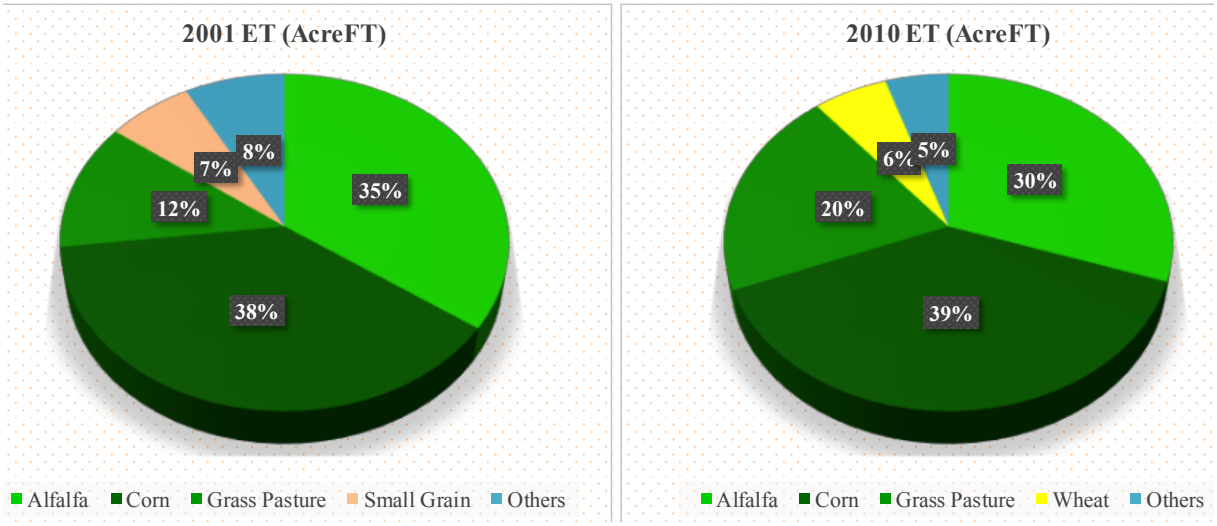

Figure 13.21. Comparison of the percentages of the *ET* of all irrigated crops for the years 2001 and 2010 of the South Platte River Basin.

Table 13.10. The area and ET of all irrigated crops and phreatophyte of the South Platte River Basin.

Crop	Area (acre)	ET (AcreFT)	avg (AF/Acre)	Area (acre)	ET (AcreFT)	avg (AF/Acre)
Alfalfa	310,521	680,263	2.19	240,049	575,485	2.40
Barley	NA	NA	NA	8,472	17,346	2.05
Blue Grass	NA	NA	NA	2,170	5,180	2.39
Corn	333,943	748,477	2.24	328,562	738,743	2.25
Dry Bans	29,401	53,465	1.82	4,775	9,203	1.93
Grass Pasture	120,073	238,595	1.99	182,600	383,209	2.10
Orchard	2,239	4,157	1.86	20	39	2.00
Small Grain	65,849	133,526	2.03	405	845	2.08
Snap Beans	NA	NA	NA	291	555	1.91
Sod Farm	5,246	10,904	2.08	35	86	2.47
Sorghum	NA	NA	NA	70	161	2.29
Sugar Beets	26,904	56,641	2.11	23,546	52,142	2.21
Sunflower	NA	NA	NA	2,639	5,097	1.93
vegetables	16,343	29,684	1.82	2,625	4,683	1.78
Wheat	NA	NA	NA	54,286	112,464	2.07
Total	910,518	1,955,712	2.15	850,546	1,905,240	2.24
Phreatophyte	201,632	404,961	2.01	201,632	412,505	2.05

Conclusions

Most of the conventional methods in estimating *ET* are based on point measurements that limit their ability to capture the spatial variability in a study area. *ET* varies spatially and seasonally according to weather and vegetation cover conditions. The hydrological models have an advantage in simulating the effects of man-induced scenarios on regional hydrology. However, considerable expertise in model use and extensive field data are required to make proper model simulations and the implementation can take several man-years. This study shows that the major advantage of applying remote sensing based evaporation procedures is that the water consumed by the soil–water–vegetation system can be derived directly without the need to quantify other complex hydrological processes. Most of the previous surface energy model (SEB) developers have recommended that these models be applied in areas having constant wind

and constant reference *ET* because they were using data for one weather station only. This can create a limitation on the application of these models in areas with high spatial variability in weather parameters. The ReSET model used in this article incorporates the spatial variability of wind and reference *ET* into the model as grids. Such an approach ensures that each cell is modeled based on its spatial location taking into consideration all the spatial variability that affects the calculation of ET. In addition, the weather station data were used while interpolating the images from the beginning to the end of the season.

References

Allen, R. G., Tasumi, M., and Trezza, R. (2005).METRIC applications manual—Version 2.0, Univ. of Idaho, Kimberly, ID.

Allen, R. G., Tasumi, M., and Trezza, R. (2007a).“Satellite-based energy balance for mapping evapotranspiration with internalized calibration (METRIC)—Applications.”J. Irrig. Drain Eng., 133(4), 395–406.

Allen, R. G., Tasumi, M., and Trezza, R. (2007b).“Satellite-based energy balance for mapping evapotranspiration with internalized calibration (METRIC)—Model.”J. Irrig. Drain Eng., 133(4), 380–394.

Bastiaanssen, W. G. M. (2000).“SEBAL based sensible and latent heat fluxes in the irrigated Gedez Basin, Turkey.”J. Hydrol. (Amsterdam), 229(1-2), 87–100.

Bastiaanssen, W. G. M., Ahmad, M. U. D., and Chemin, Y. (2002). “Satellite surveillance of evaporative depletion across the Indus Basin.” Water Resour. Res., 38(12), 91–99.

Bastiaanssen, W. G. M., *ET* al. (1998a).“Remote sensing surface energy balance algorithm for land (SEBAL): 2 Validation.” J. Hydrol. (Amsterdam), 212-213(1-4), 213–229.

Bastiaanssen, W. G. M., Menenti, M., Feddes, R. A., and Holtslag, A. A. M. (1998b).“Remote sensing surface energy balance algorithm for land (SEBAL): 1 Formulation.” J. Hydrol. (Amsterdam), 212-213(1-4), 198–212.

Beven, K.J., Wood, E.F., Sivapalan, M., 1988. On hydrological heterogeneity: catchment morphology and catchment response. J. Hydrol. 100, 353–375.

Elhaddad, A., and Garcia, L. A. (2008).“Surface energy balance-based model for estimating evapotranspiration taking into account spatial variability in weather.”J. Irrig. Drain Eng., 134(6), 681–689.

Gowda, P. H., Chavez, J. L., Colaizzi, P. D., Evett, S. R., Howell, T. A., and Tolk, J. A.□2008□. “ET mapping for agricultural water management: Present status and challenges.”Irrig. Sci.,26 (3), 223–237.

Hanson, R. L.□1991□. “Evapotranspiration and droughts.” National water summary 1988–89—Hydrologic events and floods and droughts: U.S. Geological Survey Water Supply Paper 2375, compiled by R. W. Paulson, E. B. Chase, R. S. Roberts, and D. W. Moody, USGS, Reston, Va., 99–104.

Harrison, L. P. (1963).“Fundamental concepts and definitions relating to humidity.”Chapter 3,Humidity and moisture, A. Wexler, ed., Vol. 3, Reinhold, New York, 256.

Menenti, M., and Choudhury, B. J.□1993□. “Parameterization of land surface evapotranspiration using a location dependent potential evapotranspiration and surface temperature range.”Proc., Exchange Processes at the Land Surface for a Range of Space and Time Scales, Vol. 212, Bolle H. J. et al., eds., IAHS Publ., Oxfordshire, U.K., 561–568.

Tasumi, M., Allen, R. G., Trezza, R., and Wright, J. L. (2005).“Satellitebased energy balance to assess with in-population variance of crop coefficient curves.”J. Irrig. Drain Eng., 131(1), 94–109.

Su, H., McCabe, M. F., Wood, E. F., Su, Z., and Prueger, J. H. (2005). “Modeling evapotranspiration during SMACEX: Comparing two approaches local- and regional-scale prediction.” J. Hydrometeor.,6 (6), 910–922.